AN ABSTRACT OF THE DISSERTATION OF

Ratanak So for the degree of Doctor of Philosophy in Electrical and Computer Engineering presented on April 28, 2017.

Title: Validation of Wave Energy Converter Models and the Development of Control Strategies in WEC-Sim

Abstract approved: ______________________________

Ted K.A. Brekken

When the term “renewable energy" is mentioned in a conversation, wind, solar, and hydro energy typically come to mind. However, there is one major resource that has remained mostly untapped: wave energy. Wind and solar power technologies are well established around the world but they cannot generate electricity all the time; wind is not always blowing and the sun is not always shining. An advantage of ocean wave power is that it is generally more predictable. Furthermore, water is significantly denser – about 800 times – compared to air, so it can carry more energy than wind per volume. A meter wide of incident wave front can provide about 40 kW (along the coast of Oregon or Washington) which can power about 20 homes. A coastline of length 50 km translates to 2 GW of capacity (approximately 1 million homes) which is equivalent to a large hydroelectric power plant in the U.S. The details of the work presented herein is 1) a comparison of a wave energy converter's (WEC) field test performance to a simulated expected results of the same device using WEC-Sim, an open-source simulator; 2) a comparison of a tank test performance of an oscillating water column and simulation results of a point absorber using WEC-Sim; and 3) development of model predictive control (MPC), latching & declutching, and linear quadratic Gaussian regulator (LQG) control strategies for WEC-Sim.

Validation of Wave Energy Converter Models and the Development of Control Strategies in WEC-Sim

by

Ratanak So

A DISSERTATION

submitted to

Oregon State University

in partial fulfillment of
the requirements for the
degree of

Doctor of Philosophy

Presented April 28, 2017
Commencement June 2017

Doctor of Philosophy dissertation of Ratanak So presented on April 28, 2017.

APPROVED:

Major Professor, representing Electrical and Computer Engineering

Director of the School of Electrical Engineering and Computer Science

Dean of the Graduate School

I understand that my dissertation will become part of the permanent collection of Oregon State University libraries. My signature below authorizes release of my dissertation to any reader upon request.

Ratanak So, Author

ACKNOWLEDGEMENTS

I would like to express sincere gratitude to my major advisor Prof. Ted K.A. Brekken for the continuous support of my Ph.D study and related research, for your wonderful mentoring, your passion, enthusiasm, and your immense knowledge of controls and modeling of Wave Energy Converters (WECs).

I would like to thank my committee members, Dr. Annette von Jouanne, Dr. Eduardo Cotilla-Sanchez, Dr. Julia Zhang, and Dr. Belinda Batten. Special thanks to my GCR, Dr. Janet Nishihara. The Energy Systems faculty group has been tremendous asset to me and my peers who have benefited greatly from their expertise.

In addition, I would like to thank my colleagues JiaJia Song, Mike Starrett, Ziwei Ke, Han Xiong, and Brandon Johnson for their kindness, helpfulness, time and support. It was a great honor to be their friend.

Finally, a big thank you to my family for always supporting and believing in me. Without their inspiration, encouragement and support, this achievement would not have been possible.

TABLE OF CONTENTS

Page

TABLE OF CONTENTS (Continued)

Page

LIST OF FIGURES

LIST OF FIGURES (Continued)

LIST OF FIGURES (Continued)

LIST OF TABLES

Chapter 1: Statistical Analysis of a 1:7 Scale Field Test Wave Energy Converter Using WEC-Sim

1.1 Abstract

This study uses the open-source WEC-Sim code to model the Columbia Power Technologies (CPwr) SeaRay 1:7 scale wave energy converter (WEC). WEC-Sim is intended to run quickly on standard desktop equipment and provide a very gentle learning curve for WEC modeling. This paper focuses on the linear implementation of WEC-Sim as that requires the least simulation time and is often the starting point for basic system design. WEC-Sim results are compared against the SeaRay experimental data. Two studies were conducted: a comparison of WEC-Sim predications versus experimental data across 285 trials of varying sea-states to determine overall average power and energy production; and a determination of WEC-Sim's accuracy in predicting the experimental ranges of position, speed, torque, and power. The study of average power production across many sea states shows the WEC-Sim predicts the average power of the aft float well, within 15%, but the error in the fore float is larger at 34%. The error in total predicted power is 24%. The detailed analysis of range of motion shows WEC-Sim predicted 95th percentile outliers (which dominate the design considerations) in position, speed, and torque by +15%, +14%, and +17%, respectively, for the fore float and -1%, -9%, and -6%, respectively for the aft float.

1.2 Introduction

This paper aims to evaluate the accuracy and validity of the wave energy converter (WEC) simulation tool WEC-Sim for use as an initial, fast, and easy-to-use tool for predicting energy production, positions, speeds, and torques of a complex WEC. The emphasis of the analysis is on early stage WEC development when speed, flexibility, and a short simulation time are needed to navigate a wide range of design options, as opposed to slower, more complex hydrodynamic modeling necessary for refined designs. This paper presents a comparison of experimental performance of a prototype WEC (the CPwr SeaRay) and the simulated expected results of that same WEC using WEC-Sim. The contribution of this study is to help inform WEC modelers and engineers of the current abilities and limitations of linear analysis tools, such as WEC-Sim.

Sandia National Laboratories (SNL) and the National Renewable Energy Laboratory (NREL) have jointly developed WEC-Sim, an open-source wave energy converter (WEC) design and analysis tool capable of running on a standard personal computer. WEC-Sim simulates WECs of arbitrary device geometry subject to operational and extreme waves [1]. The code is developed in MATLAB/Simulink using the multi-body dynamics solver SimMechanics, and relies on Boundary Element Method (BEM) codes to obtain hydrodynamic coefficients such as added mass, radiation damping, and wave excitation. The WEC-Sim hydrodynamic solution has been verified through code-to-code comparison, and has undergone preliminary validation through comparison to experimental data [2–5]. Furthermore, in the summer of 2016, additional validation of the WEC-Sim code with scale device tank testing was conducted at Oregon State University (OSU).

WEC-Sim was chosen because it is free, open-source, and integrated with MATLAB/Simulink, which is familiar analysis platform for many engineers. (Beside WEC-Sim, commercial softwares such as WaveDyn [6] and ProteusDS [7] – which have undergone validation against experiment – are also suited for this study.)

1.3 Wave Energy Converter Description

Columbia Power Technologies (CPwr) deployed a scaled prototype wave energy converter in the Puget Sound from February 2011 to March 2012. (The Puget Sound is a large estuary in the state of Washington in the United States and features wind-driven waves that provide a good scaled testing environment.) The SeaRay, shown in Fig. 1.1 and Fig. 1.2, consists of three rigid bodies which are constrained to move in a total of eight degrees of freedom (DOF), a nacelle (6 DOF) and two floats constrained to pitch. The

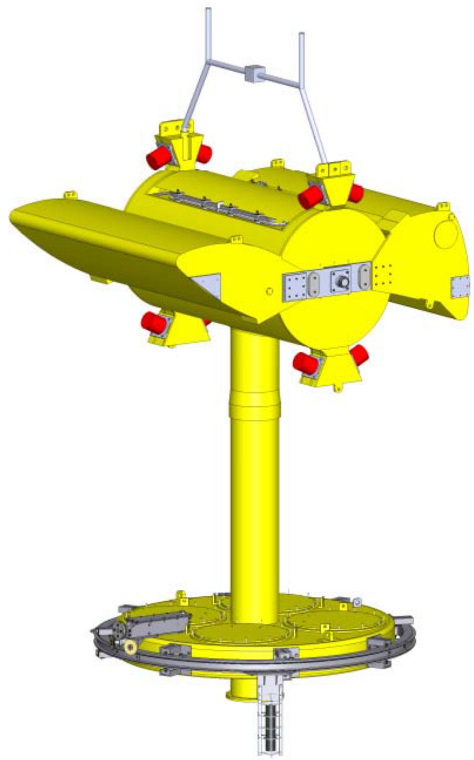

Figure 1.1: SolidWorks drawing of CPwr SeaRay 1:7 scale WEC. From left to right: fore float, nacelle, and aft float. (Image courtesy of Columbia Power Technologies.)

SeaRay is kept on station with a spread three-point mooring system, such that it can face any direction. The SeaRay prototype is a dedicated research platform instrumented with a suite of data collection equipment and sensors. The SeaRay was designed as a 1:7 scale prototype of the Generation 3.1 Ray series WEC [8].

The SeaRay is a non-symmetric point attenuator designed to operate primarily in the heave, surge, and pitch modes of motion. Non-symmetric wave energy converters have a theoretical limit of 100% capture of incident wave energy, and indeed early lab testing results of the Salter duck – which has a shape similar to the floats of the SeaRay – demonstrated capture ratios of 80% [9]. The SeaRay has a width of 2.57 meters, and during the testing period covered in this paper, operated with an average relative capture width (RCW) of 0.45. Additional information on SeaRay RCW and simulated perfor-

Figure 1.2: CPwr SeaRay 1:7 scale WEC deployed in the Puget Sound at West Point, Seattle from Feb 2011 to Mar 2012. (Image courtesy of Columbia Power Technologies.)

mance can be found in [8]. The relative pitching motion between the nacelle and either float actuates a direct drive rotary (DDR) power take off (PTO) which is the mechanism by which mechanically absorbed wave energy is converted into electrical energy. There are two separate PTOs, one linking the fore float to the nacelle and one linking the aft float to the nacelle, as shown in Fig. 1.1. The PTOs were controlled for torque linearly proportional to the rotary speed (i.e., linear damping) [10–13].

1.4 Experimental Data for Comparison

The data collected from the Puget Sound is from February 2011 to March 2012. A subset of the SeaRay data set for June 2011 is provided by CPwr for use in this study. Fore and aft generator torque, speed, and position were recorded in 512 seconds segments at a 0.04 second sample rate. The final data set for comparison is 285 trials.

Wave and current data are collected using an Acoustic Wave And Current Profiler (AWAC), allowing performance and design data to be correlated to enviromental input conditions. This data is used to characterize the metocean condition (i.e. sea states).

Several requirements are established to down-select the data. Only those trials that are

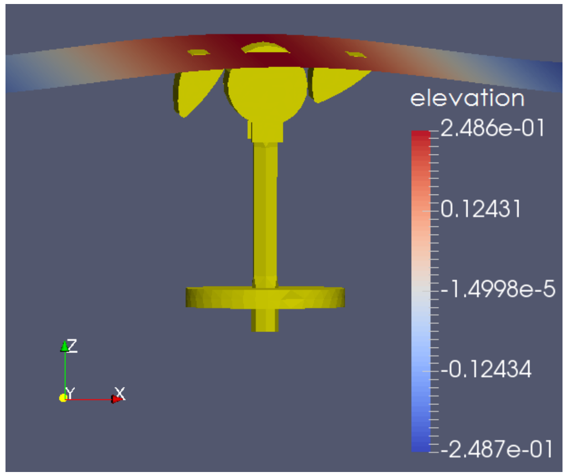

Figure 1.3: The SeaRay from the ParaView animation. From left to right: aft float, nacelle, and fore float. The wave propagates from right to left, striking the fore float first.

head on (absolute value of relative wave heading less than 22.5 degree), with relatively little directional spreading and are within the operational PTO damping cases are considered.

1.5 Simulation Setup

WEC-Sim is capable of running both linear and nonlinear hydrodynamic theories. Although the nonlinear hydrodynamic approach is available for use, the code is not efficient for running complex WEC bodies such as the SeaRay, which requires a fine mesh. The computational time is costly and it is not suited for this study. (Improvements to the non-linear capability will continue and be utilized for future research.) Other features such as viscous drag forces and mooring forces are available in WEC-Sim.

This study includes the viscous drag force calculation. The viscous drag coefficients are provided by CPWr, having been determined by prior small-scale tank testing experiments.

Mooring is not included in this study. The simulation shows that without mooring, the

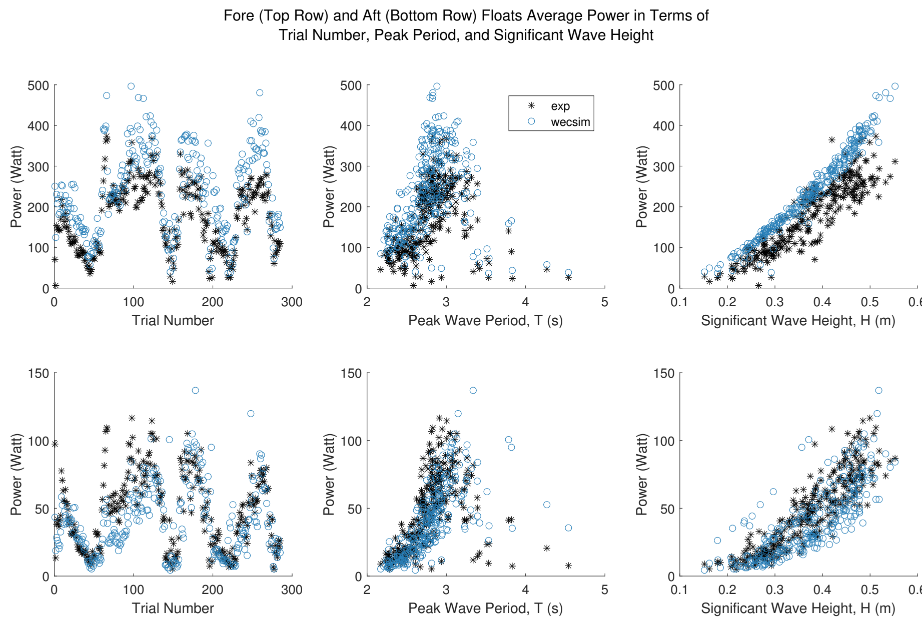

Figure 1.4: A comparison of average power in terms of trial number, peak period, and significant wave height between the experiment and WEC-Sim in the month of June 2011. The fore float results are in the top row and the aft float results in the bottom row.

WEC did drift but within an acceptable distance. CPwr used a three point mooring that connected to the damper (from top to bottom: nacelle, spar, damper). This mooring design allows vertical motion but constrains the watch circle.

Assuming linearity is also the most common initial assumption for early stage design, which is the focus of this paper. Each 1000 second simulation at 0.05 second time step typically requires 2 minutes of real time to simulate. The simulation is run with three degree-of-freedom for the nacelle (heave, surge, and pitch), and one one degree-of-freedom (pitch) for each float.

The linear model – which assumes that the body motion and the waves consist of small amplitudes in comparison to the wavelengths – uses hydrodynamics force coefficients – such as added mass, radiation damping, and wave excitation – from BEM (Boundary Element Method) tools. This approach of determining the hydrodynamic forces uses

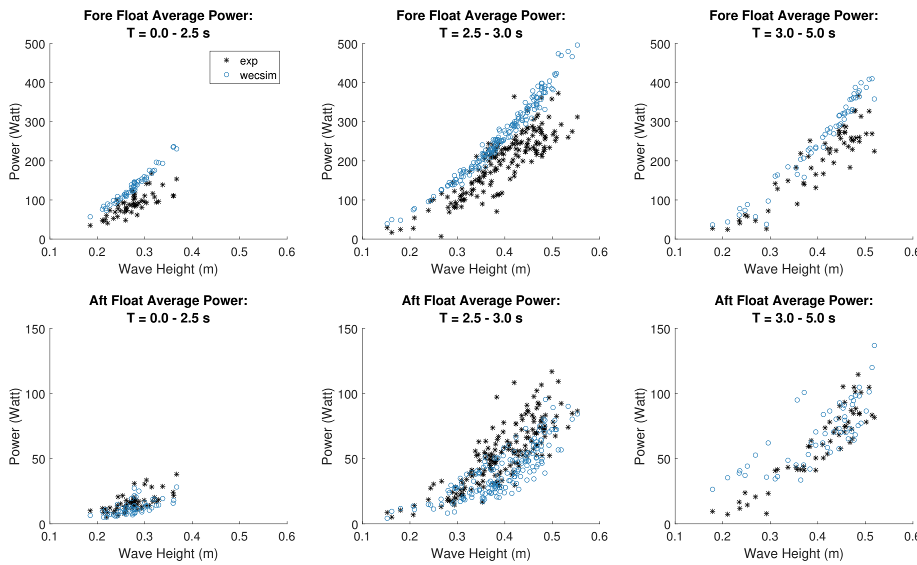

Figure 1.5: A comparison of average power in terms of wave height for three grouped wave periods: 0.0 – 2.5 seconds, 2.5 – 3.0 seconds, and 3.0 – 5.0 seconds.

the linear wave theory assumption that waves are the sum of incident, radiated, and diffracted wave components [1].

The nonlinear model – which is not used in this study – refers to the nonlinear restoring and Froude-Krylov forces when solving the system dynamics of WECs which accounting the weakly nonlinear effect on the body hydrodynamics [1].

This study accounts for body-to-body interactions when running the linear model. The body-to-body interactions refer to the interactions in the radiation force calculation in which the motion of a body causes a force on other bodies [1].

WEC-Sim models these wave forcing components using linear coefficients obtained from a frequency-domain potential flow BEM solver (e.g., WAMIT [14], AQWA-FER [15], and Nemoh [16]). The BEM solutions are obtained by solving the Laplace equation for the velocity potential, which assumes the flow is inviscid, incompressible, and irrotational.

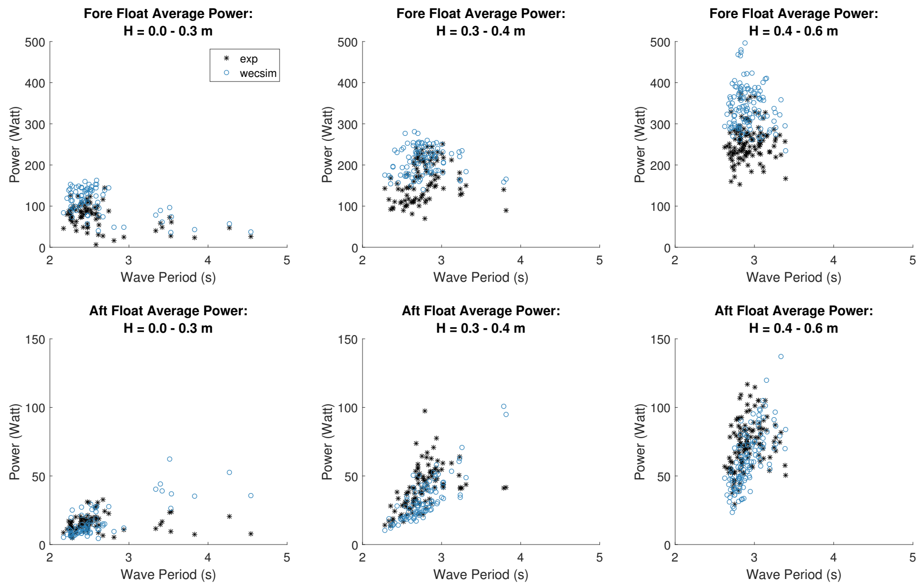

Figure 1.6: A comparison of average power in terms of wave period for three grouped wave heights: 0.0 – 0.3 meter, 0.3 – 0.4 meter, and 0.4 – 0.6 meter.

Figure 1.3 shows the SeaRay from the ParaView animation. ParaView is an open-source, multi-platform data analysis and scientific visualization application [17]. As shown in Fig. 1.3, moorings are not modeled in this study.

1.5.1 Pre-Processing

A water depth of 21 meters was used, representative of the mean observed depth during the SeaRay experiment. The surface mesh of the WEC employed a total of 10,493 diffracting panels for the BEM solution. Fig. 1.1 shows a SolidWorks drawing of 1:7 scale WEC.

The process below explains how the data is obtained from AQWA and converted into a readable file for WEC-Sim.

- AQWA – which contains information about the WEC geometry and mass properties

– produces the LIS and AH1 files that contain information about frequency-domain Boundary Element Method (BEM).

- WEC-Sim pre-processer BEMIO – developed by SNL and NREL as part of the WEC-Sim project – converts the LIS and AH1 data files to a final HDF5 format file, which is read by WEC-Sim for time-domain simulations.

1.5.2 WEC-Sim

The 285 trials selected from the experimental test data are each used to seed a comparison simulation in WEC-Sim. The process is as follows:

1. Sequentially select one of the 285 experimental test trials
2. Run a 1000 second simulation at a 0.05 second simulation step in WEC-Sim for a sea state of the same spectrum, with the same fore and aft generator damping. The spectral phase information is randomized.
3. Compare the statistical measures of generator position, speed, and torque of the experimental data versus the simulation.

The statistical measures are the absolute minimum, absolute maximum, absolute average, as well as the full probability mass functions and cumulative distribution functions.

The dynamic response of the system used in this study is calculated by solving the equation of motion for WEC systems [18, 19]. The equation of motion for a floating body, about its center of gravity, can be given as [1]:

$$m\ddot{X} = F_{ext} + F_{rad} + F_{PTO} + F_v + F_B \tag{1.1}$$

where $\ddot{X}$ can be the translational or rotational acceleration vector of the device, m is the mass matrix, F_{ext} is the wave excitation force vector, F_{rad} is the radiation force vector, F_{PTO} is the PTO force vector, F_v is the viscous drag force vector, and F_B is the net buoyancy restoring force vector.

The BEM solver is used to generate the frequency-domain forces F_{ext} and F_{rad}. The excitation term consists of a Froude-Krylov component that results from the undisturbed incident waves and a diffraction component due to the presence of the floating body. The radiation force is dependent on body acceleration and speed, represented as added-mass and damping terms. In the time domain, the frequency dependent damping component is determined via convolution with the impulse response [20].

$$F_{rad} = -A_{\infty}\ddot{X} - \int_{0}^{t} K(t-\tau)\dot{X}(\tau)d\tau \tag{1.2}$$

Where A_{∞} is the added mass matrix at infinite frequency and K is the radiation impulse response function.

The irregular excitation force is calculated as

$$F_{ext} = \Re\left[R_f \int_{0}^{\infty} F_X(\omega_r)e^{i(\omega_r t+\phi)}\sqrt{2S(\omega_r)d\omega_r}\right] \tag{1.3}$$

where S is the wave spectrum and ϕ is a random phase angle.

The PTO mechanism is represented as a linear spring-damper system, where the reaction force is given by

$$F_{PTO} = -C_{PTO}\dot{X}_{rel} \tag{1.4}$$

where C_{PTO} is the damping of the PTO.

The power of the PTO is given by:

$$P_{PTO} = -F_{PTO}\dot{X}_{rel} = C_{PTO}\dot{X}_{rel}^2 \tag{1.5}$$

The effect of viscous losses to the system is calculated as below

$$F_v = -\frac{1}{2}C_d\rho A_D\dot{X}|\dot{X}| \tag{1.6}$$

where C_d is the viscous drag coefficient, ρ is the fluid density, and A_D is the characteristic area.

1.6 Results and Discussion

The focus of the analysis is on the accuracy of WEC-Sim in assisting wave energy converter developers with two objectives: estimating average power performance (and hence revenue), and estimating system position, speed, and force (i.e., torque) to verify mechanical design constraints. Both analyses use all 285 trials of experimental data for comparison. Each trial is characterized by a significant wave height and a peak period.

1.6.1 Predicting Average Power Performance

The average power data can be presented several ways. In Fig. 1.4, the top and bottom rows present the fore and aft float average power by trial number, peak period, and significant wave height, respectively. The fore and aft float power plots on the left are plotted versus trial number. The center and right side plots are for the trials grouped by the peak wave period and significant wave height of the trial.

The results show generally good agreement, with a visually noticeable persistent over-prediction of fore float power production by WEC-Sim, and a slight under-prediction of the aft float power production. Figures 1.5 and 1.6 plot the fore and aft float average power with the trials binned by peak period and by significant wave height, respectively. Plotted this way, it is seen that the modeling errors tend to be consistent with one noticeable exception for the aft float in small, long (i.e., large period) waves. For short and medium waves, the aft float average power tended to be over-predicted, but for small, long waves there are several trials for which the aft float average power was under-predicted.

Figure 1.7 shows the average power presented in terms of sea state: peak period and significant wave height. The third column is the difference between the first two columns (i.e., WEC-Sim minus experimental). The values of the third column are given in Ta-

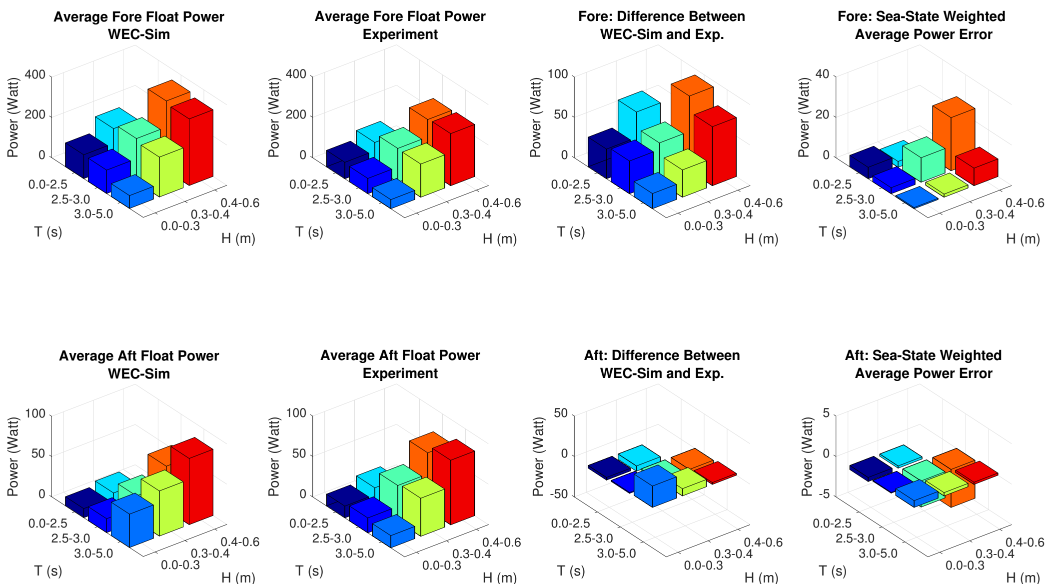

Figure 1.7: Average power presented in terms of peak period and significant wave height. A total of 285 experiment trials from June 2011 are selected for a comparison. The bars are heat-map colored according to sea state energy (i.e., red is the highest energy sea state, blue is the lowest.) The first column of plots show the WEC-Sim predicted power for the fore and aft floats by sea state. The second column shows the experimental (i.e., actual) power by sea state. The third column is the predicted power minus the experimental power (values given in Table 1.1). The fourth column is the predicted power minus the experimental power weighted by the probability mass functions of sea state (values given in Table 1.2). This illustrates the sea states for which model accuracy is most important for the purposes of predicting power performance. For both the fore and aft float, the most significant source of error is in the large height, medium length waves.

ble 1.1. Here it is very clear that the fore float power is consistently over-predicted for all sea states, and the aft float is generally under-predicted with the exception of the aforementioned small, long wave case. The largest absolute prediction error for the fore float is 92.4 W, which is 24.7% of the peak average fore float power of 374 W. The largest absolute prediction error for the aft float is 26.4 W, which is 22.6% of the peak average aft float power of 116.6 W.

Lastly the difference in prediction is weighted by the sea state probability mass function, shown in Table 1.2. Table 1.1 helps to understand the model accuracy for different

Table 1.1: Difference in Average Power (Watts) Between WEC-Sim and Exp. for Fore (white) and Aft (gray) Float

	Wave Height					
Peak Period	0.0 – 0.3 m		0.3 – 0.4 m		0.4 – 0.6 m	
0.0 – 2.5 s	36.7	-3.3	68.3	-6.5	N/A	N/A
2.5 – 3.0 s	40.5	-1.2	48.6	-13.0	92.4	-16.5
3.0 – 5.0 s	18.7	26.4	33.7	8.9	73.0	2.3

Table 1.2: Weighted Difference in Average Power (Watts) Between WEC-Sim and Exp. for Fore (white) and Aft (gray) Float

	Wave Height					
Peak Period	0.0 – 0.3 m		0.3 – 0.4 m		0.4 – 0.6 m	
0.0 – 2.5 s	5.7	-0.5	2.9	-0.3	N/A	N/A
2.5 – 3.0 s	3.0	-0.1	12.1	-3.2	26.3	-4.7
3.0 – 5.0 s	0.6	0.8	1.5	0.4	8.7	0.3

regimes, but Table 1.2 helps to understand where the model accuracy is most important for predicting overall average power (i.e., energy and hence revenue) in a realistic sea environment.

The highest sea-state weighted average power error for the fore float is 26.3 W for large height, medium length waves while the lowest is 0.6 W for small size, long waves; the total weighted fore float power error – the sum over Table 1.2 – is 60.7 W.

The highest sea-state weighted average power error for the aft float is -4.7 W for large height, medium length waves while the lowest is -0.1 W for small height, medium length waves; the total weighted aft float power error is -7.3 W.

In relative perspective, the total experimental fore float power – which is the sum over the element wise product of the PMF and the average fore float power by sea state – is 176.7 W. Therefore WEC-Sim overpredicted the fore float power by 60.7 W / 176.7 W = 34%.

The total experimental aft float power is 47.8 W. Therefore WEC-Sim underpredicted the aft float power by 7.3 W / 47.8 W = 15%

Table 1.3: Fore (white) and Aft (gray) Floats

	Fore		Aft	
	WEC-Sim	Exp.	WEC-Sim	Exp.
Position (rad)				
Mean	0.070	0.060	0.043	0.043
Std. Dev	0.058	0.051	0.039	0.039
95%ile	0.186	0.162	0.121	0.122
Velocity (rad/s)				
Mean	0.183	0.152	0.092	0.097
Std. Dev	0.150	0.137	0.081	0.093
95%ile	0.479	0.420	0.254	0.280
Torque (Nm)				
Mean	0.782e3	0.667e3	0.251e3	0.278e3
Std. Dev	0.630e3	0.541e3	0.215e3	0.228e3
95%ile	2.017e3	1.718e3	0.677e3	0.719e3
Power (Watts)				
Mean	0.237e3	0.176e3	40.641	47.751
Std. Dev	0.382e3	0.281e3	74.428	78.476
95%ile	0.964e3	0.719e3	0.171e3	0.201e3

Finally, the total weighted power error for both the fore and aft float (i.e., the total WEC power average power error) is 60.7 W - 7.3 W = 53.4 W. The total experimental fore and aft float power is 176.7 W + 47.8 W = 224.5 W. Therefore the WEC-Sim overprediction in average power is 53.4 W / 224.5 W = 24%.

1.6.2 Predicting Position, Speed, and Torque Ranges of Operation

The goal of this analysis is to ascertain the accuracy of predicting not only average power performance, but also the maximum and minimum generator position, speed, torque, and power, as these are critical limits for designing the WEC.

For example, wave energy converter designers must design the mechanical system to have a particular range of motion, the generators must be designed for a certain voltage range (which is directly related to speed), and the generators must be designed for a current range (which is directly related to torque).

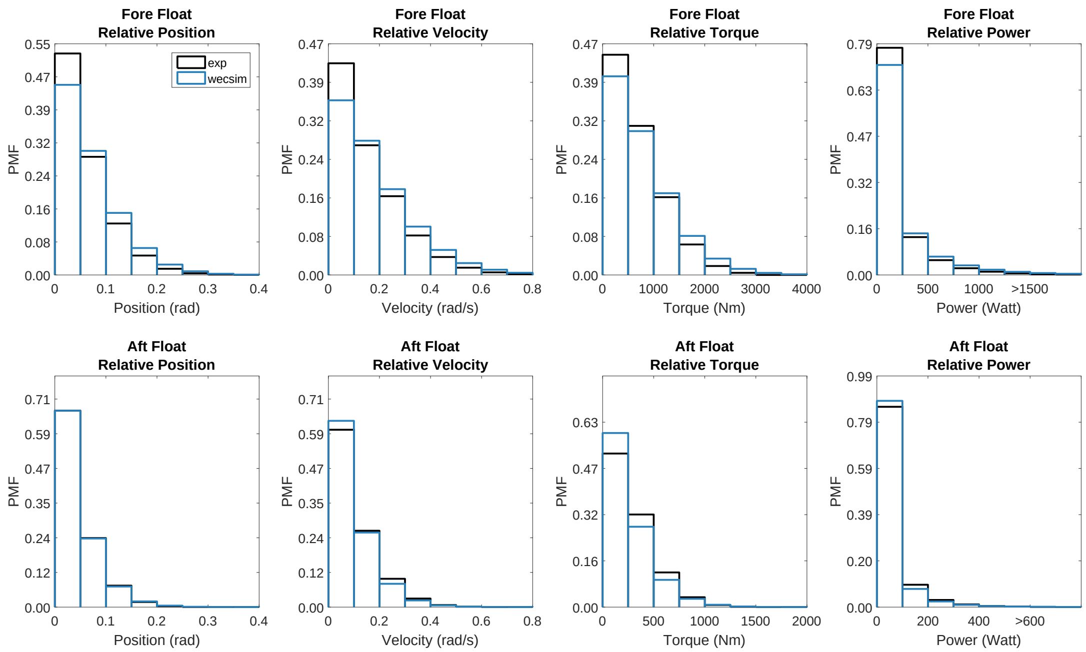

Figure 1.8: PMFs for both fore (top row) and aft floats (bottom row). Metrics for the PMFs are given in Table 1.3.

Fig. 1.8 shows the probability mass functions for the samples of the position, velocity, torque, and power time series over all 285 trials for both the experiment and the predicted WEC-Sim performance. Table 1.3 presents the mean, standard deviation, and 95th percentile (i.e., approximately 2 standard deviations away from the mean for a normal distribution).

Examining the fore float results, it is observed that there is a fairly good prediction of position and velocity. Focusing on the outlier events, the prediction error in 95th percentile position, speed, and torque is 0.186/0.162 - 1 = +15%, +14%, and +17%, respectively. For the aft float, the simulated 95th percentile predictions in position, velocity, and torque (and hence power) are -1%, -9%, and -6%, respectively.

Thus it is shown that even though WEC-Sim did not have the same exact water surface elevation profile as the actual experimental test, in a probabilistic sense, it predicted the operation of the aft float very well. On the other hand, as seen in the average power analysis WEC-Sim tends to over-predict the fore float excitation.

1.7 Conclusion

This paper presents a comparison of experimental performance of a prototype WEC (the CPwr SeaRay) and the simulated expected results of that same WEC using WEC-Sim.

The analysis focused on two key aspects: predicting long-term average power (i.e., energy) across many different sea states, and predicting instantaneous motion, torque, and power ranges. This covers two of the main uses of a tool like WEC-Sim: how much energy will be converted, and what operational limits does the WEC need to be designed for?

Considering the challenges of modeling a complex three-body device with near-field interactions using linear hydrodynamics, WEC-Sim did reasonably well in estimating the overall energy, estimating the total energy converted to within 24% (overprediction). The aft float power alone was better predicted, within 15%.

An analysis of average power by sea-state weighted by sea-state PMF shows that the primary source of prediction error for both the fore and aft float was for large height, medium length waves.

The operational ranges and limits were generally well predicted, with errors in prediction of the outliers of fore float actuation between +14% to +17%, and errors in the aft float actuation between -1% and -9%.

WEC-Sim is intended to run quickly on standard desktop equipment and provide a very gentle learning curve for WEC modeling. This paper focuses on the linear implementation of WEC-Sim as that requires the least simulation time and is often the starting point for basic system design. With linear hydrodynamics, each simulated trial of 1000 seconds requires 2 minutes of real time. With this in mind, it is shown that WEC-Sim with linear hydrodynamics gives useful first estimates of system performance, even for a complex WEC. The observed errors in prediction tended to be consistent across all operating conditions.

The possible sources of errors in prediction are off-directional or spread waves in the experimental data. This was controlled by selecting trials with head-on waves and small spreading, but there is likely some deviation present. Wave steepness and its impacts on hydrodynamics is another possible source of error. There are perhaps some indications of this in the non-consistency of predicted power for the aft float for small, long waves, which are very small steepness.

Improvements are anticipated in using WEC-Sim with non-linear hydrodynamics, at the cost of increased computation time. This is a topic for future research.

Acknowledgment

This research was made possible by support from the Wind and Water Power Technologies Office within the DOE Office of Energy Efficiency & Renewable Energy. The work was supported by Sandia National Laboratories and by the National Renewable Energy Laboratory. Sandia National Laboratories is a multi-program laboratory managed and operated by Sandia Corporation, a wholly owned subsidiary of Lockheed Martin Corporation, for the U.S. Department of Energy's National Nuclear Security Administration under contract DE-AC04-94AL85000. Special thanks to Carlos Michelen (VT), Kelley Ruehl (SNL), and Yi-Hsiang Yu (NREL) for their support on WEC-Sim.

Special thanks to Ken Rhinefrank and Pukha Lenee-Bluhm of Columbia Power Technologies (CPwr) for their support on the experimental data, and Dr. Bret Bosma (OSU) for his support on AQWA.

Chapter 2: Modeling of An Oscillating Water Column As A Point Absorber Using WEC-Sim

2.1 Abstract

This study uses the open-source WEC-Sim code to model an oscillating water column (OWC) as a point absorber. The WEC-Sim code can run quickly on a personal computer and is quite sophisticate when performing complex computation. Two studies were conducted: a comparison of WEC-Sim predictions versus experimental data for regular waves and irregular waves when the air chamber is connected to a funnel (orifice and butterfly valve). For the former, results show that for wave periods of 2.3 seconds, 2.5 seconds, and 3.3 seconds, there is a good agreement. At 1.6 second, the device is at resonance and therefore, the simulation is over-predicted. For the latter, irregular wave case, the percent error is 16% and lower for valve positions at 80°, 71°, 62°, 53°, 44°, 35°, 26°, 17°, 8°, and 24% when the valve is completely closed.

2.2 Introduction

Thousand of patents were filed in the past decades on testing their wave energy converter devices to harnessing ocean power. However, there is a small group that tested their device on the open sea. Among these wave energy converters is an oscillating water column device [21–24].

This paper aims to investigate if an oscillating water column can be modeled as a point absorber. The simulation tool used in this paper is an open-source WEC-Sim (Wave Energy Converter-SIMulator) code. The code is written using MATLAB/Simulink platform and is the result of the U.S. Department of Energy's Water Power Technologies Office funding. It is developed by a collaboration between the National Renewable Energy

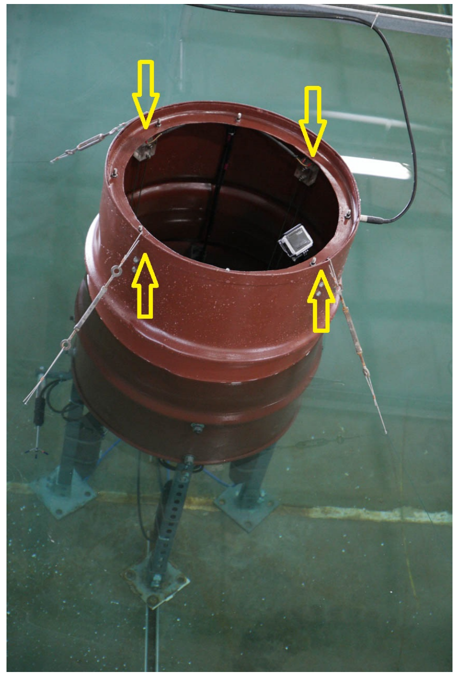

Figure 2.1: The prototype of an oscillating water column device when the air chamber is open. As waves approach, the water inside the chamber rises. As waves retreat, the water inside the chamber drops. The arrows show the location of the four wave gauges used for recording the water surface elevation inside the chamber.

Laboratory (NREL) and Sandia National Laboratories (SNL).

This paper presents a comparison of experimental performance of an oscillating water column and simulated expected results of a point absorber. The contribution of this study is to address any concern whether modeling an oscillating water column as a point absorber is a good assumption. It also provides an insight to help inform WEC controllers and engineers of the current abilities and limitation of this device.

The WEC-Sim code has been verified through code-to-code comparison, and has undergone preliminary validation through comparison to experimental data [2–5]. Additionally, validation of the WEC-Sim code with scaled device tank testing was performed at Oregon State University (OSU) in the summer of 2016.

WEC-Sim was chosen because it is a free, open-source, and integrated with MAT-

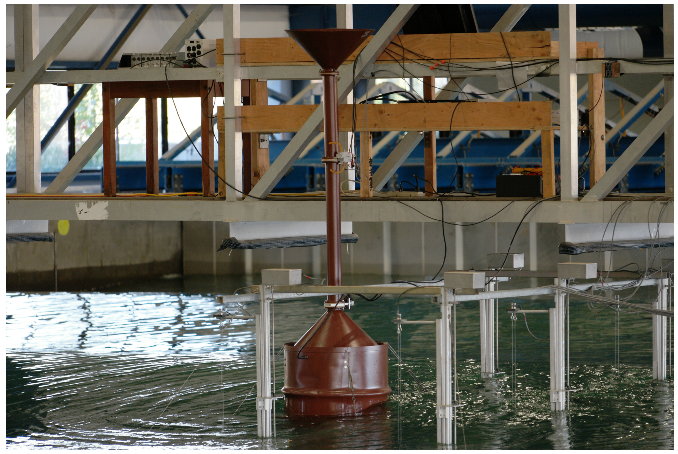

Figure 2.2: The prototype of the oscillating water column device when the funnel is connected to the air chamber.

LAB/Simulink, which is a familiar analysis platform for many engineers. (Beside WEC-Sim, commercial softwares such as WaveDyn [6] and ProteusDS [7] – which have undergone validation against experiment – are also suited for this study.)

2.3 Oscillating Water Column Description

An oscillating water column is an air chamber with an opening to the water [25], [26]. The upper portion of the chamber is connected to a funnel (an orifice and butterfly valve). As waves arrive, water is forced into the chamber and the air is compressed. As the water drops below the water line, air is then drawn back from the atmosphere through the funnel and into the chamber [25], [26].

Figures 2.1 and 2.2 show a prototype used for the experimental tank testing used in this study. Fig. 2.1 also show where all four wave guages located at. Fig. 2.2 show the set up used in this study, where the air chamber is connected to a funnel.

To help explain the difference between the tank testing and the simulation, Fig. 2.3 is shown. There are two external forces, the wave excitation force and PTO force. In the tank testing, the PTO force is the product of pressure and the cross-sectional area of the

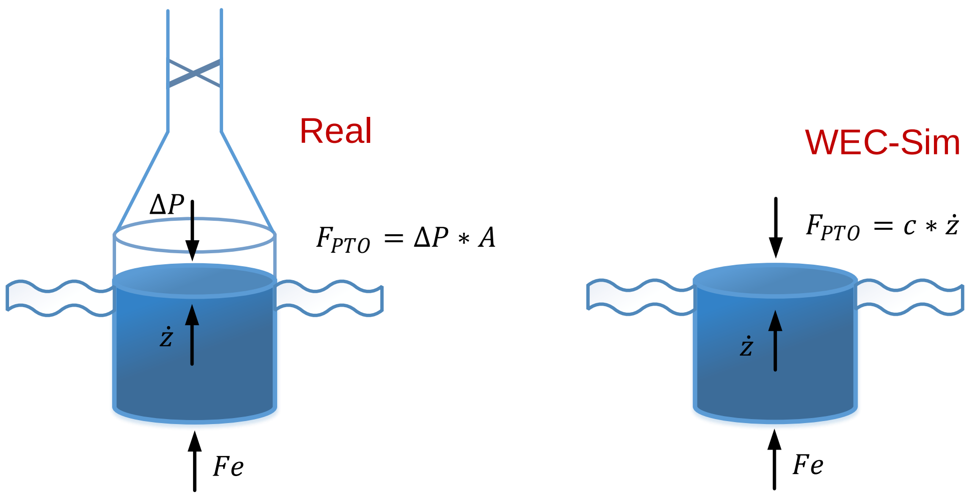

Figure 2.3: The representation of an oscillating water column device. As waves approach, the water inside the chamber rises and compress air. As waves retreat, the water drops and air is pulled into the chamber. Top represents an oscillating water column used in the experiment, and bottom (a point absorber) is used in WEC-Sim.

chamber. In order to model PTO force in WEC-Sim, the PTO damping available from the experiment is needed. PTO force in the simulation is defined as the product of PTO damping and water surface velocity of the chamber.

2.4 Experimental Setup

There are four wave gauges attached to the inside of the chamber to measure the water surface elevation as shown in Fig. 2.1. The average of the four wave guages is used in this study for a comparison against simulation. This study discusses two cases: 1) regular wave case and 2) irregular wave case. For both of these cases the air chamber is connected to the funnel. The wave periods and wave height used in this study are the operational wave profiles.

Case 1: Regular wave case.

- Run regular waves with the same wave height of 0.136 meter at wave periods 1.2

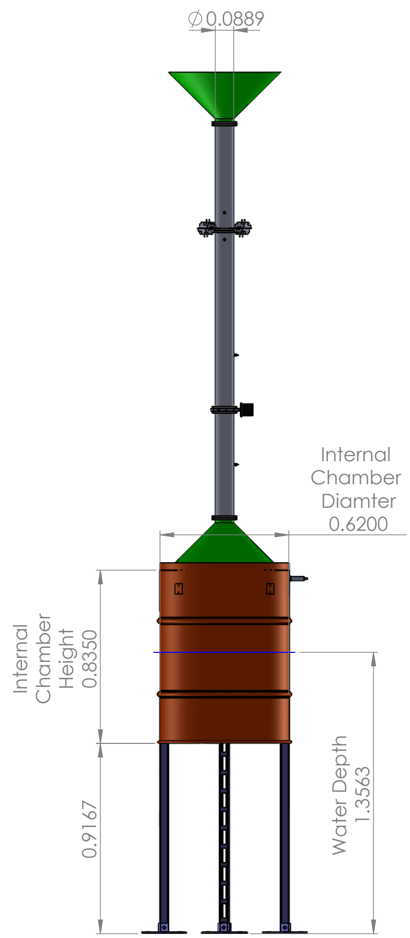

Figure 2.4: Oscillating water column device schematic.

second, 1.6 seconds, 1.9 second, 2.3 seconds, 2.6 second, and 3.3 seconds.

Case 2: Irregular wave case.

- Run irregular waves with the same wave significant wave height of 0.136 meter and wave peak period of 2.6 seconds.
- Run a total of 10 valve positions: 80°, 71°, 62°, 53°, 44°, 35°, 26°, 17°, 8°, and 0°.

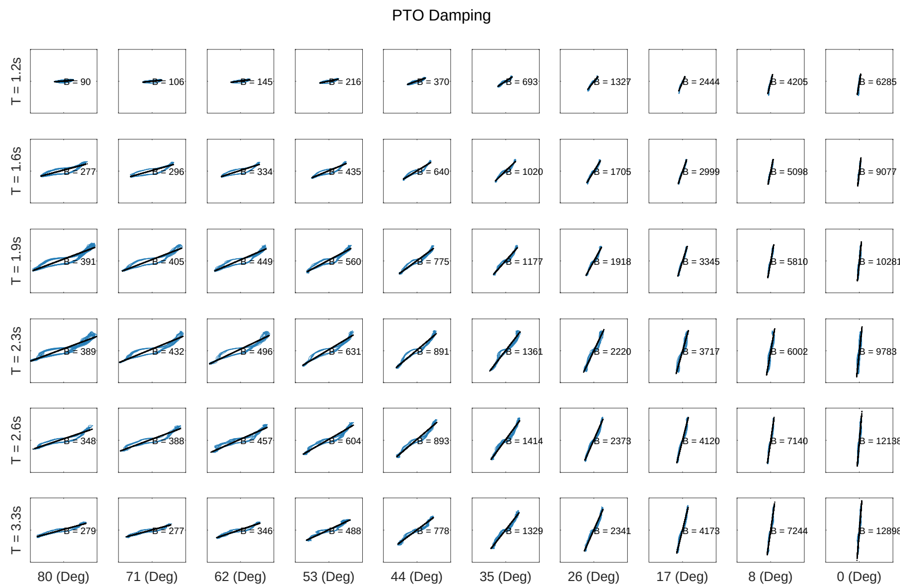

Figure 2.5: PTO damping approximation. Each plot represents the pressure differential times the chamber cross sectional area versus the device velocity. The slopes (black lines) are used as the PTO damping values in WEC-Sim.

2.5 Simulation Setup

WEC-Sim is capable of running both linear and nonlinear hydrodynamic theories. Although the nonlinear hydrodynamic approach is available for use, this study uses the linear approach. Other features such as viscous drag forces and mooring forces are available in WEC-Sim. This study does not include the viscous drag force and does not need to model the mooring since the physical device does not require.

Assuming linearity is also the most common initial assumption for early stage design, which is the focus of this paper.

For irregular waves, each 1600 seconds simulation at 0.01 second time step typically requires about 3 minutes of real time to simulate. The simulation is run with one degree-of-freedom (heave direction) for the body.

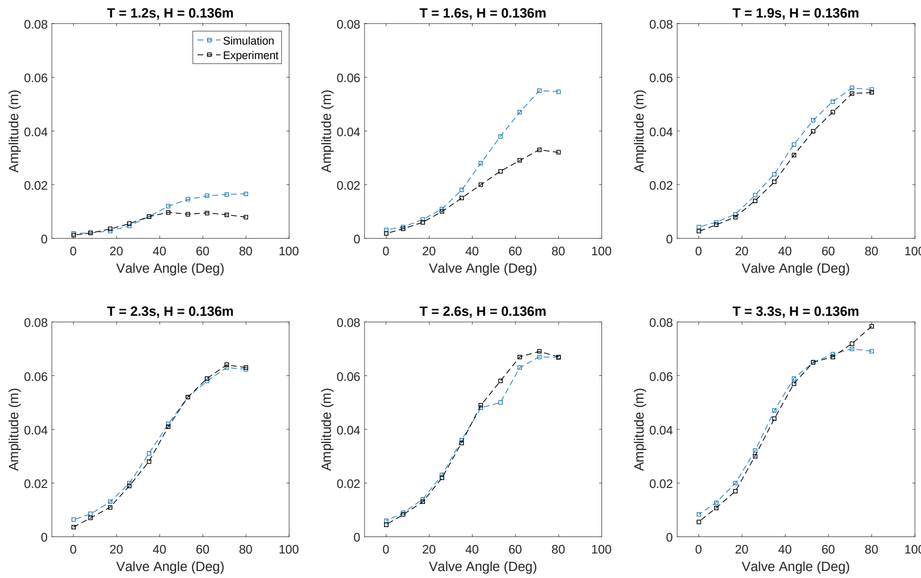

Figure 2.6: A comparison of regular wave amplitude as a function of wave period and valve position. For the same valve position, long waves yield higher amplitude. When the valve angle is larger, the amplitude is increasing.

The linear model – which assumes that the body motion and the waves consist of small amplitudes in comparison to the wavelengths – uses hydrodynamics force coefficients – such as added mass, radiation damping, and wave excitation – from BEM (Boundary Element Method) tools. This approach of determining the hydrodynamic forces uses the linear wave theory assumption that waves are the sum of incident, radiated, and diffracted wave components [1].

The nonlinear model – which is not used in this study – refers to the nonlinear restoring and Froude-Krylov forces when solving the system dynamics of WECs which accounting the weakly nonlinear effect on the body hydrodynamics [1].

WEC-Sim models these wave forcing components using linear coefficients obtained from a frequency-domain potential flow BEM solver (e.g., WAMIT [14], AQWA-FER [15], and Nemoh [16]). The BEM solutions are obtained by solving the Laplace equation for the velocity potential, which assumes the flow is inviscid, incompressible, and irrota-

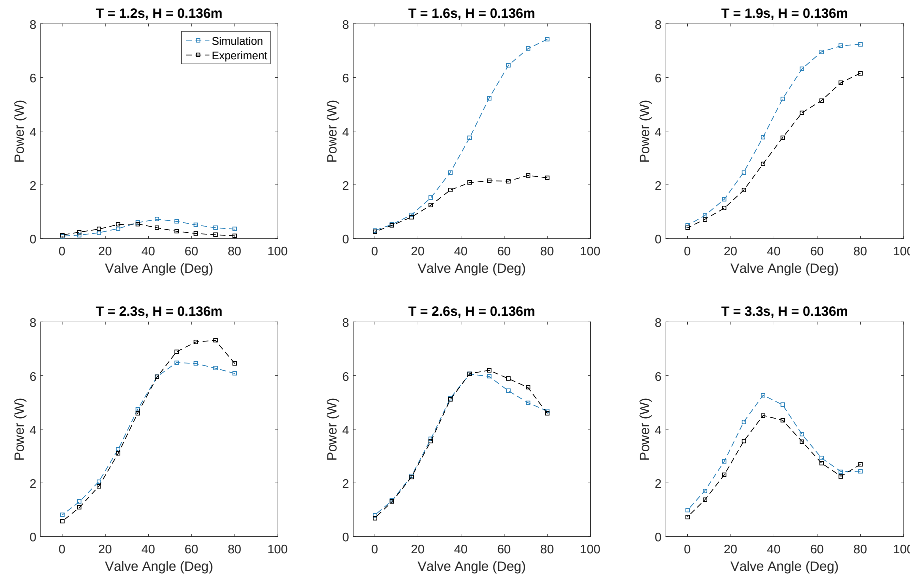

Figure 2.7: A comparison of regular wave average power as a function of wave period and valve position. For the same valve position, long waves yield higher power. When the valve angle is larger, the power is increasing.

tional.

2.5.1 Pre-Processing

A water depth of 1.3563 meters was used, representative of the mean observed depth during the oscillating water column experiment.

The process below explains how the data is obtained from AQWA and converted into a readable file for WEC-Sim.

- AQWA – which contains information about the WEC geometry and mass properties – produces the LIS and AH1 files that contain information about frequency-domain Boundary Element Method (BEM).
- WEC-Sim pre-processer BEMIO – developed by SNL and NREL as part of the

WEC-Sim project – converts the LIS and AH1 data files to a final HDF5 format file, which is read by WEC-Sim for time-domain simulations.

2.5.2 WEC-Sim

The same wave height, period, and PTO damping from the experiment as shown in Fig. 2.5 is used for regular waves.

The same significant wave height, wave peak period, wave spectrum, and PTO damping selected from the experimental test data are each used to seed a comparison simulation in WEC-Sim.

The process is as follows:

1. Sequentially select one of the experimental test trials
2. Run a 1600 second simulation at a 0.01 second simulation step in WEC-Sim for a sea state of the same spectrum, with damping values from the experiment. The spectral phase information is randomized.
3. Compare the statistical measures of the water surface position in the chamber from the experimental data versus the simulation.

The statistical measures are the absolute minimum, absolute maximum, absolute average, as well as the full probability mass functions and cumulative distribution functions.

The dynamic response of the system used in this study is calculated by solving the equation of motion for WEC systems [18, 19]. The equation of motion for a floating body, about its center of gravity, can be given as [1]:

$$m\ddot{Z} = F_{ext} + F_{rad} + F_{PTO} + F_B \tag{2.1}$$

where $\ddot{Z}$ is the translational acceleration vector of the device, m is the mass matrix, F_{ext} is the wave excitation force vector, F_{rad} is the radiation force vector, F_{PTO} is the PTO force vector, and F_B is the net buoyancy restoring force vector.

The BEM solver is used to generate the frequency-domain forces F_{ext} and F_{rad}. The excitation term consists of a Froude-Krylov component that results from the undisturbed incident waves and a diffraction component due to the presence of the floating body. The radiation force is dependent on body acceleration and speed, represented as added-mass and damping terms. In the time domain, the frequency dependent damping component is determined via convolution with the impulse response [20].

$$F_{rad} = -A_{\infty}\ddot{Z} - \int_{0}^{t} K(t-\tau)\dot{Z}(\tau)d\tau \tag{2.2}$$

Where A_{∞} is the added mass matrix at infinite frequency and K is the radiation impulse response function.

The irregular excitation force is calculated as

$$F_{ext} = \Re\left[R_f \int_{0}^{\infty} F_Z(\omega_r)e^{i(\omega_r t+\phi)}\sqrt{2S(\omega_r)d\omega_r}\right] \tag{2.3}$$

where S is the wave spectrum and ϕ is a random phase angle.

The PTO mechanism is represented as a linear spring-damper system, where the reaction force is given by

$$F_{PTO} = -C_{PTO}\dot{Z} \tag{2.4}$$

where C_{PTO} is the damping of the PTO.

2.6 Results and Discussion

2.6.1 Case 1: Regular Waves

Figure 2.6 shows a comparison of regular wave amplitude between the simulation and experiment. Except at the resonance period of 1.6 second, modeling an oscillating water column as a point absorber seems to have a good agreement. When the waves frequency

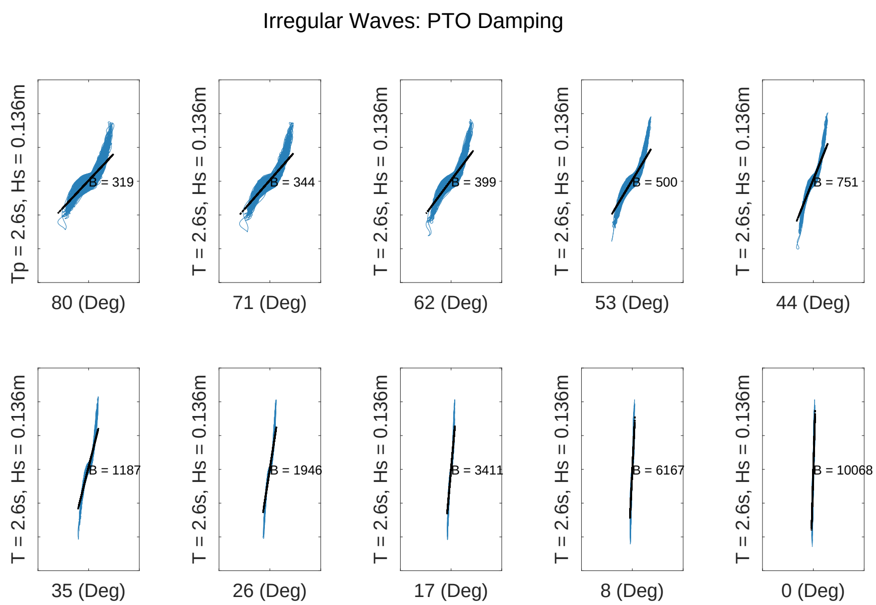

Figure 2.8: PTO damping for irregular waves.

matches a device resonance frequency, it yields a bigger response. Therefore, it is expected to see the result from WEC-Sim is higher than the experiment at the resonance period of 1.6 second. Wave period of 1.2 second can be considered as fast waves and modeling an oscillating water column as a point absorber is not valid.

It is also important to consider how much power this oscillating water column can generate. Figure 2.7 shows a power comparison. For wave period of 2.3 seconds, 2.6 seconds, and 3.3 seconds, the experimental average power peaks at 71°, 53°, and 35°, respectively.

2.6.2 Case 2: Irregular Waves

The PTO damping for the irregular wave case is shown in Fig. 2.8. Peak period of 2.6 seconds and significant wave height of 0.136 meter is used for all valve positions.

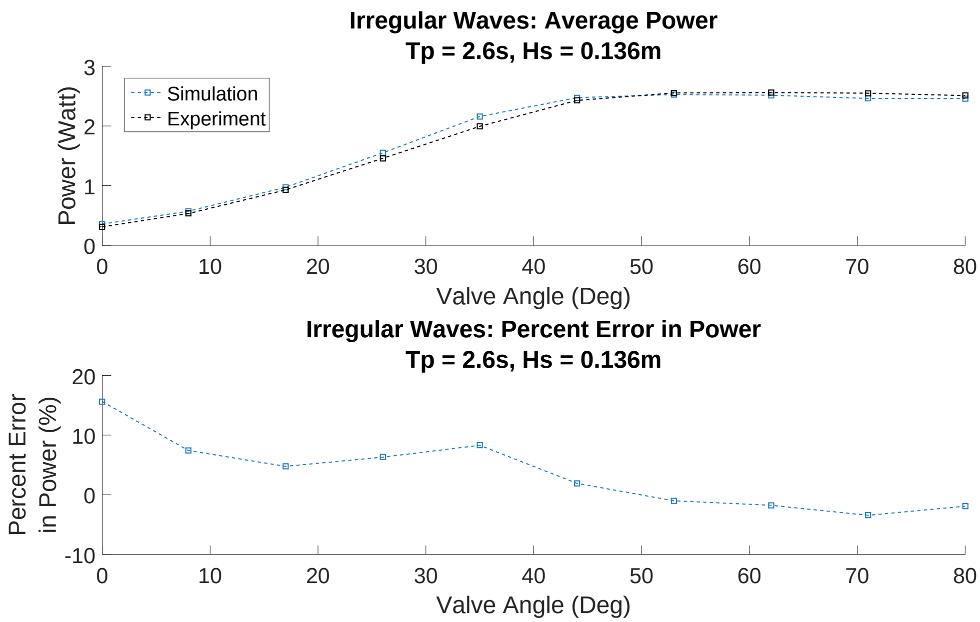

Figure 2.9: Power and percent error in power of irregular waves.

Figure 2.9 show the average power and percent error in power. When the valve is completely closed, the error in power is about 16%. When the valve is opened, the highest error is 8%. These results seem to indicate that modeling an oscillating water column as a point absorber could actually work.

Figures 2.10 and 2.11 show the probability mass functions and cumulative distribution functions for the samples of the power time series over 10 valve angles for both the experiment and the predicted WEC-Sim performance. The results indicate some agreement between the experiment and WEC-Sim. Focusing on the outlier events, the power errors in 95th percentile (100*(simulation/experiment - 1)) for valve angles at 80°, 71°, 62°, 53°, 44°, 35°, 26°, 17°, 8°, and 0° are -11%, -16%, -14%, -9%, -6%, 9%, 11%, 16%, 14%, and 23%, respectively. These results also agree with the finding for percent error in power above. Only when the valve is closed the error is high, the rest is 16% and lower.

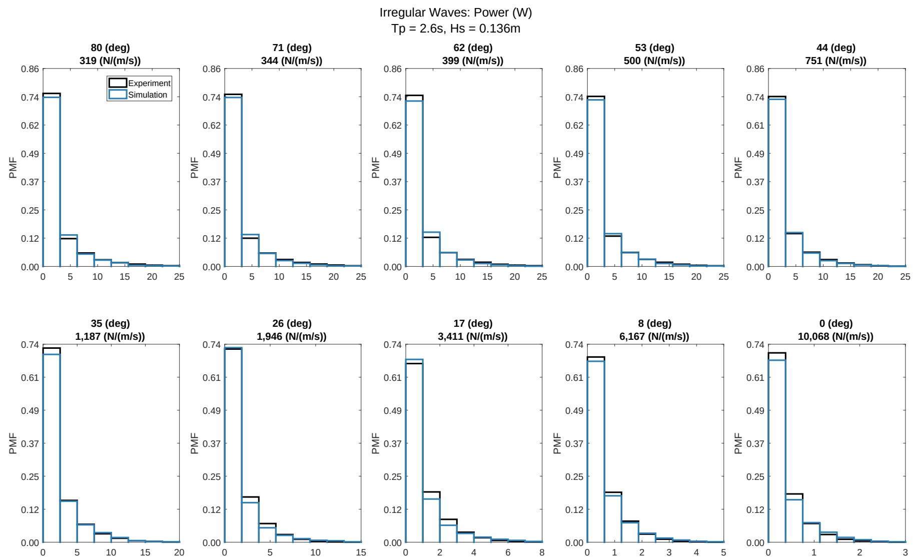

Figure 2.10: PMFs for irregular waves.

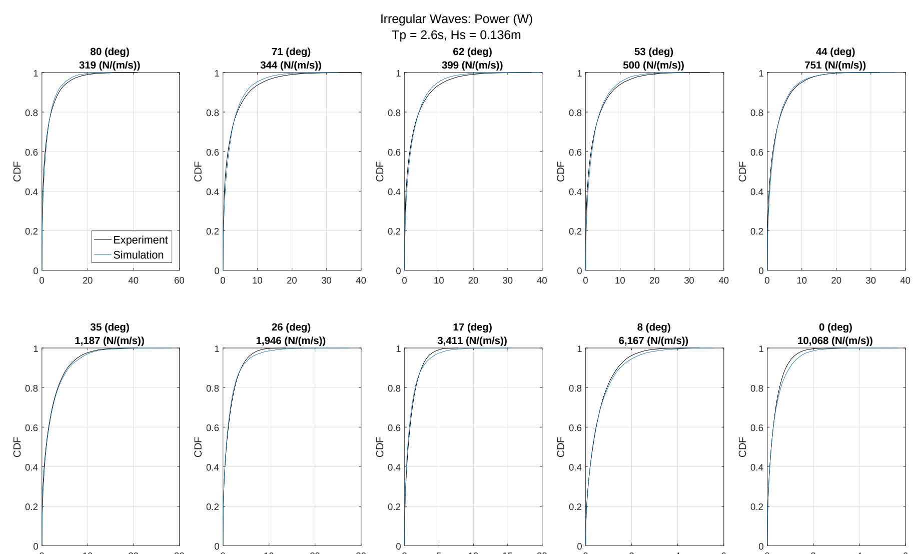

Figure 2.11: CDFs for irregular waves.

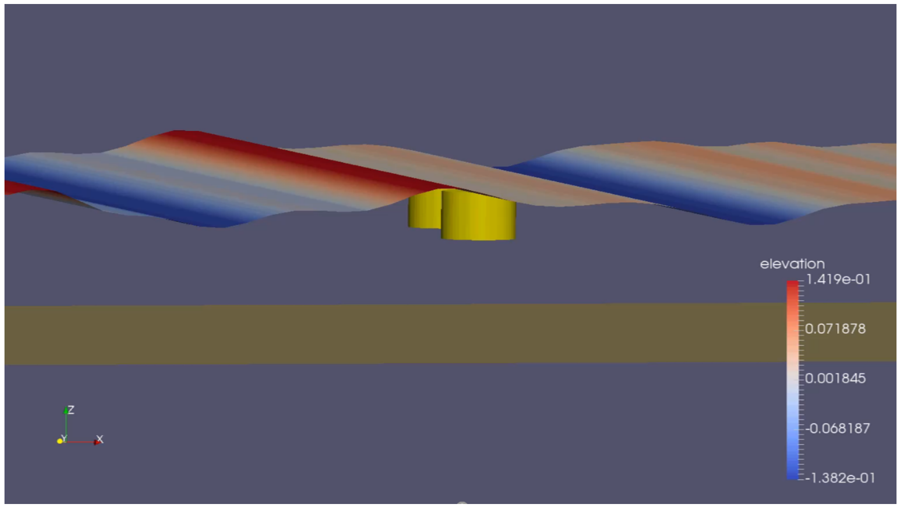

Figure 2.12: Two bodies.

2.7 Body to Body Interactions

For a single body WEC, the force equation is shown below. For control purpose, a state-space representation is shown in 2.6.

$$F_e + F_r + F_b + F_{pto} = m\ddot{z} \tag{2.5}$$

$$\frac{d}{dt}\begin{bmatrix} \dot{z} \\ z \\ F_r' \\ \int_{-\infty}^{t} F_r'\, d\tau \end{bmatrix} = \begin{bmatrix} 0 & \frac{-k}{m+A(\infty)} & \frac{1}{m+A(\infty)} & 0 \\ 1 & 0 & 0 & 0 \\ -\frac{c_{aa}}{c_{ba}} & -\frac{c_{ab}}{c_{ba}} & -\frac{c_{bb}}{c_{ba}} & -\frac{c_{bc}}{c_{ba}} \\ 0 & 0 & 1 & 0 \end{bmatrix} \begin{bmatrix} \dot{z} \\ z \\ F_r' \\ \int_{-\infty}^{t} F_r'\, d\tau \end{bmatrix} + \begin{bmatrix} \frac{1}{m+A(\infty)} \\ 0 \\ 0 \\ 0 \end{bmatrix} \begin{bmatrix} F_{pto} \end{bmatrix} + \begin{bmatrix} \frac{1}{m+A(\infty)} \\ 0 \\ 0 \\ 0 \end{bmatrix} \begin{bmatrix} F_e \end{bmatrix} \tag{2.6}$$

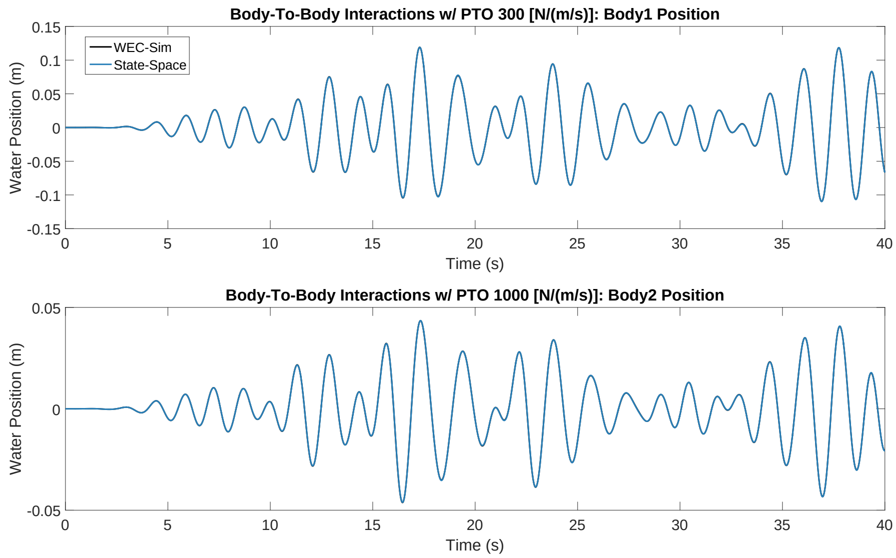

Figure 2.13: Body 1 and body 2 position. Body 1 uses PTO damping of 300 (Ns/m) while body 2 used PTO damping of 1000 (Ns/m).

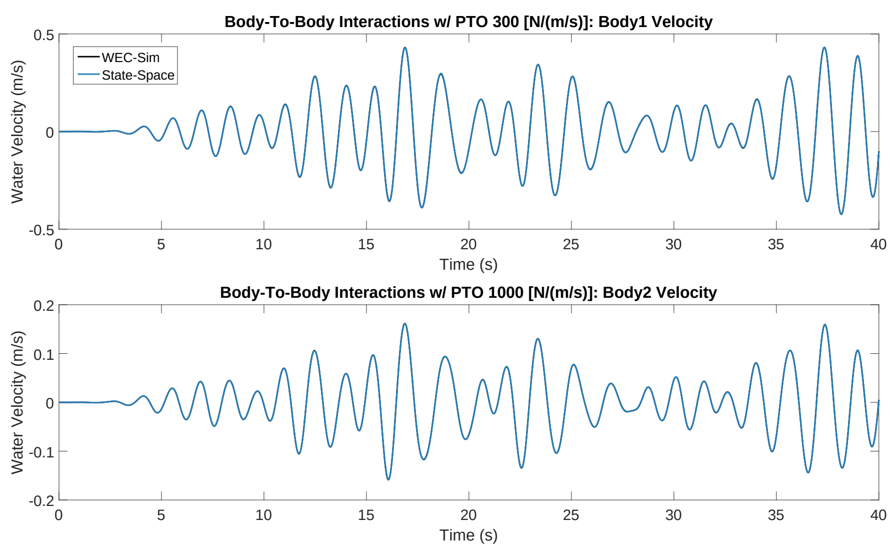

Figure 2.14: Body 1 and body 2 velocity.

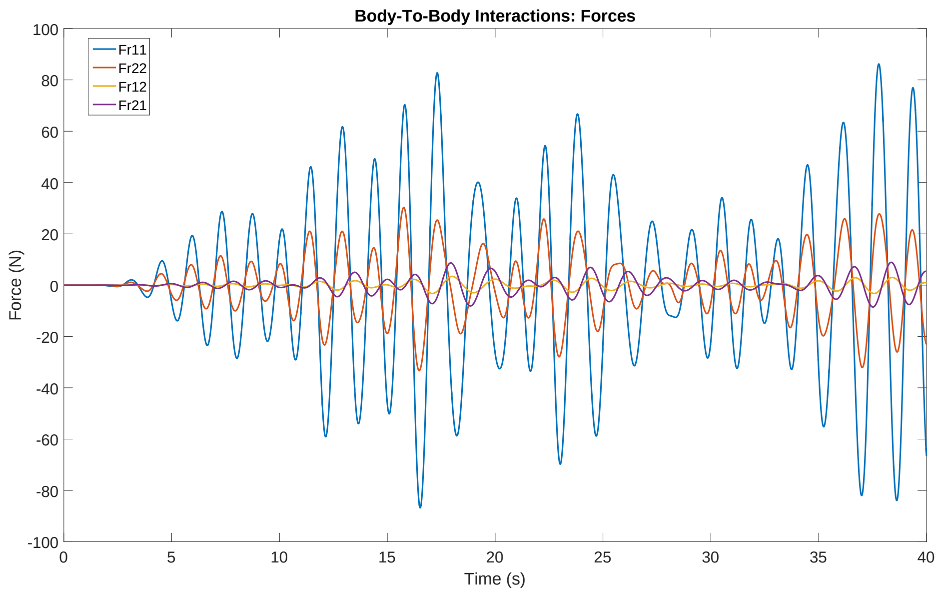

Figure 2.15: Body-to-body interactions forces. Body 1 uses PTO damping of 300 (Ns/m) while body 2 used PTO damping of 1000 (Ns/m). F_{r11} is the self radiation for body 1. F_{r22} is the self radiation for body 2. F_{r12} is the cross term due to motion of body 2 on body 1. F_{r21} is the cross term due to motion of body 1 on body 2.

$$F_{e1} + F_{r11}(\ddot{z}_1, \dot{z}_1) + F_{r12}(\ddot{z}_2, \dot{z}_2) + F_{b1}(z_1) + F_{PTO1} = m_1\ddot{z}_1 \tag{2.7}$$

$$F_{e2} + F_{r22}(\ddot{z}_2, \dot{z}_2) + F_{r21}(\ddot{z}_1, \dot{z}_1) + F_{b2}(z_2) + F_{PTO2} = m_2\ddot{z}_2 \tag{2.8}$$

When two bodies is next to each other, it is important to understand the significant of their interactions. The interaction between bodies is a WEC system is manifested as a cross-coupled radiation force. F_{r12} is the radiation force on body 1 due to motion of body 2. Equations 2.7 and 2.8 below show the relationship between body 1 and 2. Fig. 2.15 shows all the forces for two bodies. F_{r11} which has a small damping of 300 (Ns/m) is the biggest force. Therefore, it is expected to see F_{r21} bigger than F_{r12}. From this plot, it is clear that the cross terms are significant and cannot be neglected.

A state-space model for two bodies is compared against a convolution method in WEC-

Sim. Results show that the state-space is very accurate. Therefore, the state-space can be used for control.

2.8 Conclusion

This paper investigates if a point absorber can be used as a model for an oscillating water column. After comparing the simulation against the experiment, the study concludes that a point absorber can be used as a representation of the oscillating water column.

This paper focuses on the responses of the oscillating water column for 1) regular waves, and 2) irregular waves. The former test presents both the amplitude and average power. The latter test show the average power, percent error in power, probability mass functions, and cumulative distribution functions. Focusing on the outlier events, the power errors in 95th percentile for valve angles at 80°, 71°, 62°, 53°, 44°, 35°, 26°, 17°, 8°, and 0° are -11%, -16%, -14%, -9%, -6%, 9%, 11%, 16%, 14%, and 23%, respectively. These results also agree with the finding for percent error in power above. Only when the valve is closed the error is high, the rest is 16% and lower. A state-space model for two bodies including the body-to-body interactions was compared to the convolution approach. Results indicate that the state-space model is valid.

Acknowledgment

This research was made possible by support from the Wind and Water Power Technologies Office within the DOE Office of Energy Efficiency & Renewable Energy. The work was supported by Sandia National Laboratories and by the National Renewable Energy Laboratory. Sandia National Laboratories is a multi-program laboratory managed and operated by Sandia Corporation, a wholly owned subsidiary of Lockheed Martin Corporation, for the U.S. Department of Energy's National Nuclear Security Administration under contract DE-AC04-94AL85000.

Special thanks to Dr. Bret Bosma (OSU) for his support on AQWA.

Chapter 3: Development of Control-Sim: Control Strategies for Power Take-Off Integrated Wave Energy Converter

3.1 Abstract

In recent years, Sandia National Laboratories (SNL) and the National Renewable Energy Laboratory (NREL) have jointly developed an open-source wave energy converter code known as WEC-Sim (Wave Energy Converter-Simulator); capable of simulating WECs of arbitrary device geometry subject to both operational and extreme waves. However, this code does not include control which has the potential to optimize power. Because of this, there has been interest in having an open-source control that works with the code. The first part of this paper lays out the development of Control-Sim which is designed to support the WEC-Sim code. Control strategies discuss in this paper include linear spring damping, latching & declutching, linear quadratic Gaussian regulator (LQG), and model predictive control (MPC). The second part demonstrates a comparison between linear damping and energy optimization MPC using WEC-Sim coupled with Control-Sim.

3.2 Introduction

There are several control strategies that can be integrated with WEC to optimize power production. Fig. 3.1 illustrates the top level of WEC with control and PTO block. Control-Sim takes the WEC system dynamic states (including the knowledge of excitation force) and calculates the (optimal energy) desired PTO force. This force is passed on to PTO-Sim (Power Take Off-Simulator). Then, the PTO-Sim block outputs the PTO force back into the WEC plant model.

Candidates for Control-Sim could be linear spring damper, complex conjugate, latching

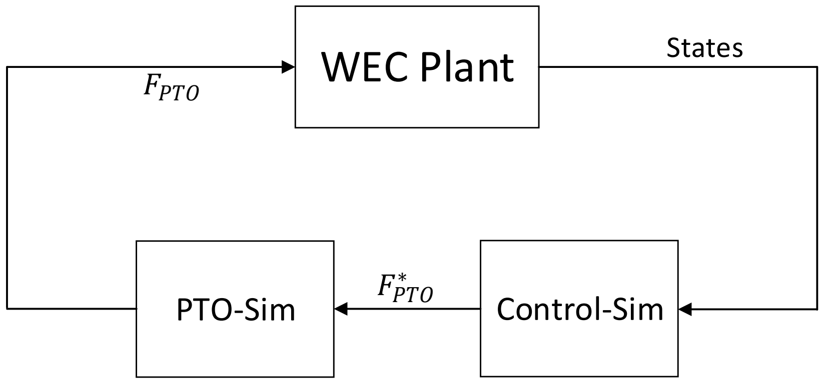

Figure 3.1: Top level control diagram.

and declutching, LQG, and MPC.

Options for PTO-Sim could be ideal, hydraulic, and direct drive generator (linear or rotary). PTO-Sim could also have its own low level control such as PIDs (Proprotional-Intregral-Derivative). For example, PIDs could be used to control motor/generator speed or torque and voltage or current of a hydraulic PTO or a direct drive linear/rotary generator, respectively.

3.3 Control Strategies for WEC

The following discusses different control approaches for WEC.

3.3.1 Linear Damping

A simple control for a power take-off force is to model this force as a linear spring-damper system.

$$F_{PTO} = -K_{PTO}X_{rel} - C_{PTO}\dot{X}_{rel} \tag{3.1}$$

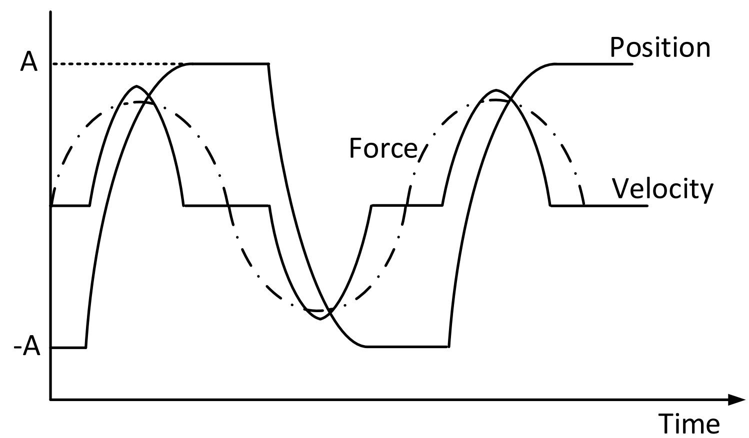

Figure 3.2: Latching control.

where K_{PTO} is the stiffness of the PTO, C_{PTO} is the damping of the PTO, and X_{rel} and $\dot{X}_{rel}$ are the relative motion and velocity between two bodies [1]. In this case F^{*}_{PTO} is F_{PTO} since PTO-Sim is ideal.

3.3.2 Latching and Declutching

This control strategy is basically implemented by turning on and off PTO force [27]. For latching operation, the WEC uses the PTO where its PTO damping term is modeled using a general sigmoid function [28]. In other words, the damping is a function of maximum and minimum boundaries, time delay, and damping slope. Fig. 3.2 shows the latching operation.

For declutching operation, the WEC does not use PTO. Salter et al. [29] and Wright et al. [30], consider declutching control as “freewheeling." For declutching, the PTO force is zero.

When latching and declutching are combined, the conversion allows the WEC to increase its power capture performance. For simplicity, linear damping can be used as its PTO in this case. The goal for the control strategy is for the buoy velocity to be in phase with the excitation force. As a result, the overall energy capture is increased. This control method is suitable only for incident waves with periods larger than the resonant period of the WEC body. For irregular waves, the concept of phase between excitation force and velocity is not trivial, in which case the objective of optimization of the latching interval is not unique. So, the latching time can be optimized to synchronize the peak of the velocity with the peak of the excitation force. Unlike optimal complex conjugate control, latching and declutching do not use the reactive power concept – therefore this strategy can be less complicated when implementing.

3.3.3 Linear Quadratic Gaussian Regulator (LQG)

The LQG uses the state feed feedback approach for designing optimal regulators [31]. The LQG controller normally has an optimal state feedback gain and a Kalman state estimator. The top level block diagram is shown in Fig. 3.3. The optimal feedback gain is calculated such that the following performance index below is minimized.

$$J = \int_0^\infty (x^T Q x + u^T R u) dt \tag{3.2}$$

The feedback control law can be written as follows:

$$u = -Fx \tag{3.3}$$

where Q and R are positive definite or semi-definite Hermittian or real symmetric matrices. The output of the WEC system (state measurement) is used as an input to the Kalman filter. This filter estimates the buoy speed and position.

$$\hat{x} = \begin{bmatrix} \hat{x_1} & \hat{\dot{x_1}} \end{bmatrix} \tag{3.4}$$

The LQG controller contains the Kalman state estimator in addition to optimal state feedback gains. These states are multiplied by the corresponding optimal gains to produce the control signals necessary to generate the optimal PTO force.

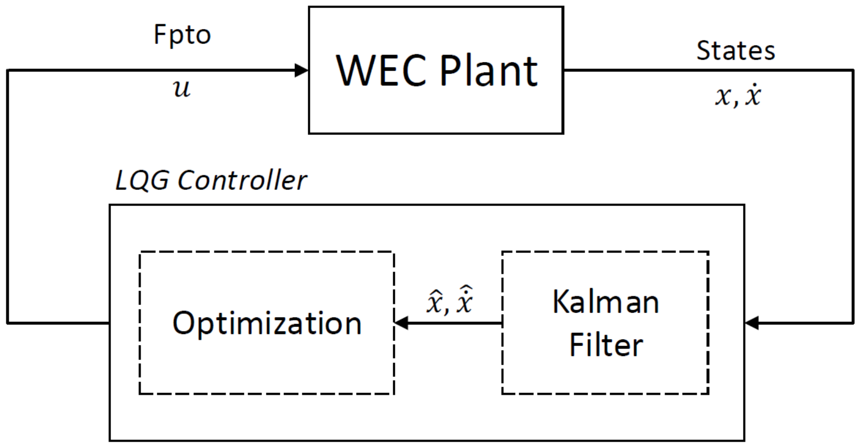

Figure 3.3: LQG Controller coupled with the WEC plant model.

3.3.4 Complex Conjugate Control

The energy maximization approach can be achieved by using the force-to-velocity relationship below [32]:

$$F_e(s) + F_{PTO}(s) = Z_i(s)V(s) \tag{3.5}$$

where $Z_i(s)$ is the mechanical intrinsic impedance. The power take-off force F_{PTO} is assumed to have components proportional to vertical acceleration, vertical velocity, and vertical position.

$$F_{PTO}(s) = Z_{PTO}(s)V(s) \tag{3.6}$$

$$F_e(s) = (Z_i(s) - Z_{PTO}(s))V(s) \tag{3.7}$$

Since power is force times velocity, optimal power capture by the power take-off becomes an impedance-matching problem.

$$Z_{PTO,OPT}(s) = -Z_i^*(s) \tag{3.8}$$

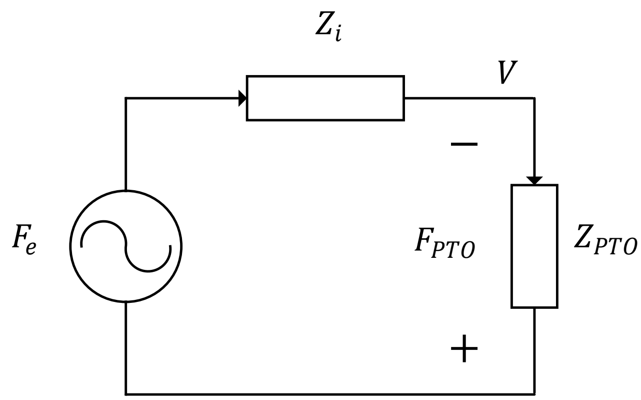

Figure 3.4: Impedance matching analogous to electrical circuit for optimal control.

The impedance-matching problem is well understood by many (electrical) engineers. So, the analogy of force to voltage, velocity to current, and mechanical impedance to electrical impedance. An analogous equivalent circuit is shown in Fig. 3.4.

The optimal power can be achieved when Z_{PTO} is $-Z_i^*$, which means the PTO mass and spring cancel the actual mass and spring terms. Therefore, the power take-off damping term is the actual float radiation damping.

$$\begin{aligned} F_{PTO,OPT}(s) &= Z_{PTO,OPT}(s)V(s) \\ &= -Z_i^*(s)V(s) \end{aligned} \tag{3.9}$$

The optimal control law can be specified in terms of the desired velocity $V_{OPT}(s)$.

$$\begin{aligned} F_e(s) &= Z_i(s)V_{OPT}(s) - F_{PTO,OPT} \\ &= (Z_i(s) + Z_i^*(s))V_{OPT}(s) \\ &= 2Re\{Z_i(s)\}V_{OPT}(s) \end{aligned} \tag{3.10}$$

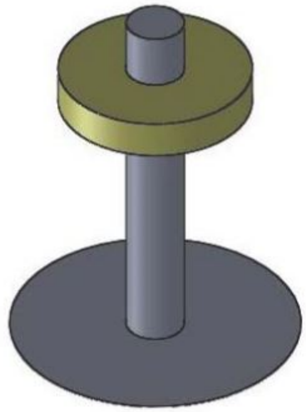

Figure 3.5: Reference Model 3. (Image courtesy of WEC-Sim)

$$V_{OPT}(s) = \frac{1}{2Re\{Z_i(s)\}} F_e(s) \tag{3.11}$$

The condition in (3.11) is a condition on the amplitude of $V_{OPT}(s)$, with the restriction that $V_{OPT}(t)$ be in phase with $F_e(t)$, since $Re\{Z_i(s)\}$ is a real (and even) function. This phase condition, considered separately, forms the basis for some simple WEC phase control strategies, such as latching [27].

3.4 Model Predictive Control with WEC-Sim

The following discussions of MPC focus mainly on the cost function and soft constraints. Details of this work on estimation of measurement states can be found from [33] [34].

3.4.1 Plant Model

For a simplified model of WEC as showed in Fig.3.5, this study uses linear wave theory and the equation of motion is

$$F_e(t) + F_r(t) + F_b(t) + F_{PTO}(t) = m\ddot{z}(t) \tag{3.12}$$

Where F_e is the excitation force, F_r is the radiation force, F_b is the buoyancy force, and F_{PTO} is the power take off force [35].

The state space representation of the WEC motion using the dependent radiation force can be shown below:

$$\frac{d}{dt}\begin{bmatrix} \dot{z} \\ z \\ F_r' \\ \int_{-\infty}^{t} F_r' \\ F_{PTO} \end{bmatrix} =$$

$$\underbrace{\begin{bmatrix} 0 & \frac{-k}{m+A(\infty)} & \frac{1}{m+A(\infty)} & 0 & \frac{-k}{m+A(\infty)} \\ 1 & 0 & 0 & 0 & 0 \\ -\frac{c_{aa}}{c_{ba}} & -\frac{c_{ab}}{c_{ba}} & -\frac{c_{bb}}{c_{ba}} & -\frac{c_{bc}}{c_{ba}} & 0 \\ 0 & 0 & 1 & 0 & 0 \\ 0 & 0 & 0 & 0 & 0 \end{bmatrix}}_{\mathbf{A}} \begin{bmatrix} \dot{z} \\ z \\ F_r' \\ \int_{-\infty}^{t} F_r' \\ F_{PTO} \end{bmatrix}$$

$$+ \underbrace{\begin{bmatrix} 0 \\ 0 \\ 0 \\ 0 \\ 1 \end{bmatrix}}_{\mathbf{Bu}} \begin{bmatrix} \dot{F}_{PTO} \end{bmatrix} + \underbrace{\begin{bmatrix} \frac{1}{m+A(\infty)} \\ 0 \\ 0 \\ 0 \\ 0 \end{bmatrix}}_{\mathbf{Bv}} \begin{bmatrix} F_e \end{bmatrix} \tag{3.13}$$

$$\frac{d}{dt}\mathbf{x}(t) = \mathbf{A}\mathbf{x}(t) + \mathbf{B}_u\mathbf{u}(t) + \mathbf{B}_v\mathbf{v}(t) \tag{3.14}$$

$$\mathbf{y}(t) = \mathbf{C}\mathbf{x}(t) + \mathbf{D}_u\mathbf{u}(t) + \mathbf{D}_v\mathbf{v}(t) \tag{3.15}$$

After discretization, we will have

$$\mathbf{x}(k+1) = \mathbf{A}\mathbf{x}(k) + \mathbf{B}_u\mathbf{u}(k) + \mathbf{B}_v\mathbf{v}(k) \tag{3.16}$$

$$\mathbf{y}(k) = \mathbf{C}\mathbf{x}(k) + \mathbf{D}_u\mathbf{u}(k) + \mathbf{D}_v\mathbf{v}(k) \tag{3.17}$$

Recursive substitution yields

$$\overrightarrow{\mathbf{y}}(k) = \mathbf{S}_x\mathbf{x}(k) + \mathbf{S}_u\overrightarrow{\mathbf{u}}(k) + \mathbf{S}_v\overrightarrow{\mathbf{v}}(k) \tag{3.18}$$

Where

$$\overrightarrow{\mathbf{y}}(k) = \begin{bmatrix} \mathbf{y}(k) \\ \mathbf{y}(k+1) \\ \mathbf{y}(k+2) \\ \mathbf{y}(k+3) \\ \vdots \\ \mathbf{y}(k+H_p) \end{bmatrix}, \mathbf{S}_x = \begin{bmatrix} \mathbf{C} \\ \mathbf{CA} \\ \mathbf{CA}^2 \\ \mathbf{CA}^3 \\ \vdots \\ \mathbf{CA}^{H_p} \end{bmatrix} \tag{3.19}$$

$$\mathbf{S}_{u,v} = \begin{bmatrix} \mathbf{D}_{u,v} & 0 & 0 & 0 & \cdots & 0 \\ \mathbf{CB}_{u,v} & \mathbf{D}_{u,v} & 0 & 0 & \cdots & 0 \\ \mathbf{CAB}_{u,v} & \mathbf{CB}_{u,v} & \mathbf{D}_{u,v} & 0 & \cdots & 0 \\ \mathbf{CA}^2\mathbf{B}_{u,v} & \mathbf{CAB}_{u,v} & \mathbf{CB}_{u,v} & \mathbf{D}_{u,v} & \cdots & 0 \\ \vdots & \vdots & \vdots & \vdots & \ddots & \vdots \\ \mathbf{CA}^{H_p-1}\mathbf{B}_{u,v} & \mathbf{CA}^{H_p-2}\mathbf{B}_{u,v} & \cdots & \cdots & \mathbf{CB}_{u,v} & \mathbf{D}_{u,v} \end{bmatrix} \tag{3.20}$$

$$\overrightarrow{\mathbf{u}}(k) = \begin{bmatrix} \mathbf{u}(k) \\ \mathbf{u}(k+1) \\ \mathbf{u}(k+2) \\ \mathbf{u}(k+3) \\ \vdots \\ \mathbf{u}(k+H_p) \end{bmatrix}, \overrightarrow{\mathbf{v}}(k) = \begin{bmatrix} \mathbf{v}(k) \\ \mathbf{v}(k+1) \\ \mathbf{v}(k+2) \\ \mathbf{v}(k+3) \\ \vdots \\ \mathbf{v}(k+H_p) \end{bmatrix} \tag{3.21}$$

3.4.2 Optimization Function

For the predictive model in (3.18), we can define the following cost function:

$$J(k) = \frac{1}{2}\vec{\mathbf{y}}(k)^T\mathbf{Q}\vec{\mathbf{y}}(k) + \frac{1}{2}\vec{\mathbf{u}}(k)^T\mathbf{R}\vec{\mathbf{u}}(k) \tag{3.22}$$

Where it is then re-formulated to a linear quadratic programing form:

$$\begin{aligned} J(k) = {} & \frac{1}{2}\vec{\mathbf{u}}(k)^T \underbrace{(\mathbf{S_u}^T\mathbf{Q}\mathbf{S_u} + \mathbf{R})}_{\mathbf{H}} \vec{\mathbf{u}}(k) \\ & + \vec{\mathbf{u}}(k)^T \underbrace{\mathbf{S_u}^T\mathbf{Q}(\mathbf{S_x}\mathbf{x}(k) + \mathbf{S_v}\vec{\mathbf{v}}(k))}_{\boldsymbol{f}} \end{aligned} \tag{3.23}$$

Where $\mathbf{Q}$ can be chosen to select speed times force terms, in which case the cost function is energy. If $\mathbf{S_u}^T\mathbf{Q}\mathbf{S_u}$ is not positive semidefinite, then the cost function is non convex. This issue can be fixed by designing the $\mathbf{R}$ matrix such that $\mathbf{H}$ is a positive semidefinite. For example, let $\mathbf{R} = rI$, where I is the identity matrix. To make sure $\mathbf{H}$ is a positive semidefinite, then the value of r needs to be greater than the negative minimum of $eig(\mathbf{S_u}^T\mathbf{Q}\mathbf{S_u})$. In other words, if the minimum eigenvalue is -1, then r should be greater than 1. Since $\mathbf{H}$ is now a positive semidefinite, then the cost function is convex. The $\mathbf{R}$ matrix also plays a role as to penalize the rate of change of PTO force.

Subject to

$$\begin{bmatrix} \mathbf{I} \\ -\mathbf{I} \\ \mathbf{S}_u \\ -\mathbf{S}_u \end{bmatrix} \begin{bmatrix} \vec{\mathbf{u}}(k) \end{bmatrix} \leq \begin{bmatrix} \vec{\mathbf{u}}_{upperbound} \\ -\vec{\mathbf{u}}_{lowerbound} \\ \vec{\mathbf{y}}_{upperbound} - \mathbf{S}_x\mathbf{x}(k) - \mathbf{S}_v\vec{\mathbf{v}}(k) \\ -\vec{\mathbf{y}}_{lowerbound} + \mathbf{S}_x\mathbf{x}(k) + \mathbf{S}_v\vec{\mathbf{v}}(k) \end{bmatrix} \tag{3.24}$$

Thus (3.23) and (3.24) are the standard quadratic programming formulation

$$\min J(x) = \frac{1}{2}x^T Hx + f^T x \tag{3.25}$$

Subject to

$$Ax \leq b \tag{3.26}$$

$$A_{eq}x = b_{eq} \tag{3.27}$$

3.4.3 Hard Constraints

A constraint of the form given in (3.24) is considered a hard constraint. The convex optimization solver must find a solution which meets all constraints or the problem is considered infeasible; the solver has no flexibility to find the best possible solution which violates a constraint. If the problem is infeasible, the last known good PTO force can be applied (from a previous MPC solution), or the solver may be run again with a new relaxed constraint matrix, or some other manually programmed strategy may be employed.

3.4.4 Soft Constraints Through Slack Variables

A soft constraint has an initial value for all constraints which can be widened (i.e., softened) by the solver during runtime if necessary to find a feasible solution. Soft constraints can be implemented by augmenting the objective to include new, high cost slack variables for the control input, the output states, or both. In the latter case, the energy optimizing MPC formulation given in (3.22) is re-written as

$$\begin{aligned} J_{soft}(k) = & \frac{1}{2}\overrightarrow{\mathbf{y}}(k)^T\mathbf{Q}\overrightarrow{\mathbf{y}}(k) + \frac{1}{2}\overrightarrow{\mathbf{u}}(k)^T\mathbf{R}\overrightarrow{\mathbf{u}}(k) \\ & + \frac{1}{2}\overrightarrow{\boldsymbol{\delta}_u}(k)^T\mathbf{W}_u\overrightarrow{\boldsymbol{\delta}_u}(k) + \frac{1}{2}\overrightarrow{\boldsymbol{\delta}_y}(k)^T\mathbf{W}_y\overrightarrow{\boldsymbol{\delta}_y}(k) \end{aligned} \tag{3.28}$$

Where the slack variable $\boldsymbol{\delta}_u$ represents the ability to soften the constraint on the control input $\overrightarrow{\mathbf{u}}(k)$, and the matrix $\mathbf{W}_u$ is chosen to place a high cost on doing so. The slack variable $\boldsymbol{\delta}_y$ is used and scaled likewise to soften constraints on $\overrightarrow{\mathbf{y}}(k)$.

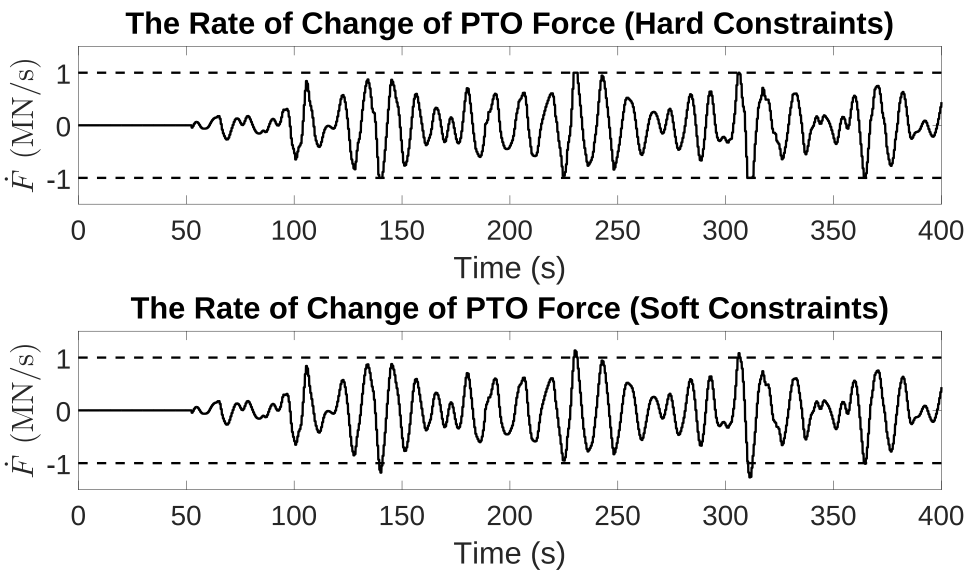

Figure 3.6: The rate of change of PTO force using hard and soft constraints.

3.4.5 WEC-Sim Simulation Result

A Reference Model 3 (RM3) two-body point absorber WEC – the DOE-funded Reference Model Project – is used in this study [36]. Fig. 3.6 was simulated using JONSWAP wave spectrum with a peak period of 12 seconds and a significant wave height of 2.5 meters. It represents the rate of change of PTO force using hard constraints (top) and soft constraints (bottom).

Table 3.1: Average Power (kWatts) Between MPC (white) and Fixed Damping (gray)

	Height							
Period	1.5 m		2.0 m		2.5 m		3.0 m	
5 s	10.3	12.3	18.3	21.9	28.6	34.2	41.2	49.2
7 s	28.3	33.5	50.4	59.5	79.6	93.0	116	134
9 s	31.2	29.2	56.1	52.0	89.4	81.2	132	117
11 s	56.5	23.1	102	41.1	160	64.2	229	92.5
13 s	111	20.3	194	36.0	294	56.3	409	81.1

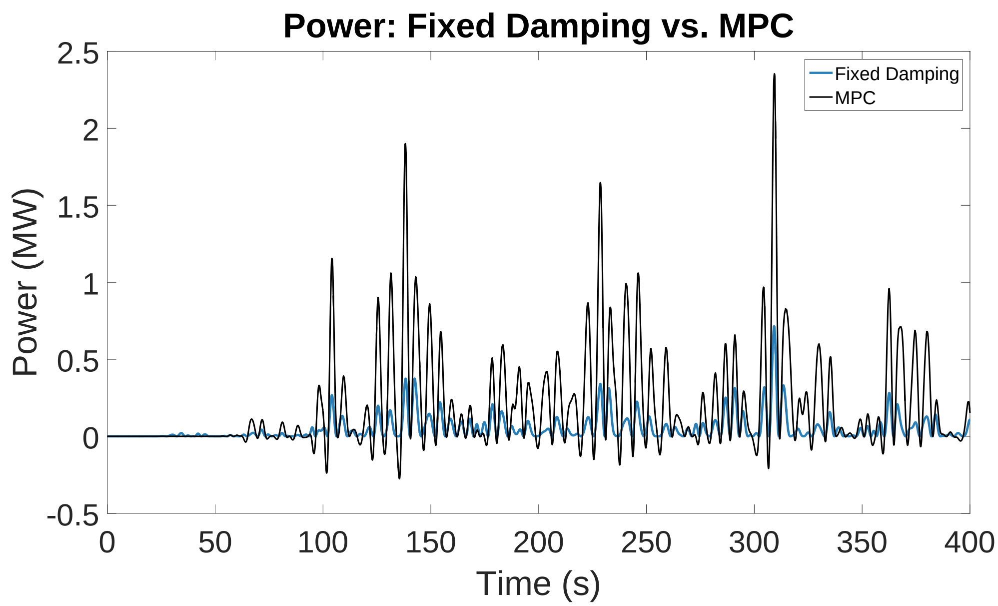

Figure 3.7: Power comparison using soft constraints.

Figure 3.7 compares the instantaneous power between fixed damping and MPC. The MPC approach allows the WEC to take advantage of reactive power.

Figure 3.8 demonstrates the MPC average power and fixed damping average power for different sea states. The details of the average power for different sea states can be found in Table 3.1. The MPC approach can capture higher power when the wave is long and energetic. For short and small waves, the MPC average power does not out perform the fixed damping approach. These results show that improvements in average power capture of up to 500% vs. fixed damping are achievable without exceeding the device constraints.

3.4.6 Body-To-Body Interactions

This section presents an advanced feature where the body-to-body interactions are included. In other words, both the float and spar are allowed to moved in heave direction. The affects of float on spar and spar on float are accounted in the force calculation.

Figure 3.9 shows the top level diagram of an integrated MPC with WEC-Sim. MPC has a plant model and a control model. The plant model as shown in Fig. 3.10 show the state-space representation of hydrodynamics. Fig. 3.11 shows the excitation force prediction for float and spar, the states, and MPC function. MPC function uses the knowledge of prediction, the states, constraints, and calculates the optimal rate of change of PTO force trajectory.

To confirm that the state-space representation of MPC is valid, Figs. 3.12 and 3.13 show both float and spar motion. This verification is done by applying the same PTO force, which calculated from MPC, to both the WEC-Sim and the MPC state-space.

3.5 Conclusion

This paper discusses different control strategies and how they can optimize power for wave energy converters. Some techniques such as latching and declutching are simpler to model and do not use reactive power while MPC, on the other hand, has a higher power capture improvement but requires the use of reactive power.

Acknowledgment

This research was made possible by support from the Wind and Water Power Technologies Office within the DOE Office of Energy Efficiency & Renewable Energy. The work was supported by Sandia National Laboratories. Sandia National Laboratories is a multi-program laboratory managed and operated by Sandia Corporation, a wholly owned subsidiary of Lockheed Martin Corporation, for the U.S. Department of Energy's National Nuclear Security Administration under contract DE-AC04-94AL85000. Special thanks to Kelley Ruehl (SNL) for her support on WEC-Sim.

Special thanks to Dr. Mike Starrett (Northwest Power and Conservation Council) for his support on MPC.

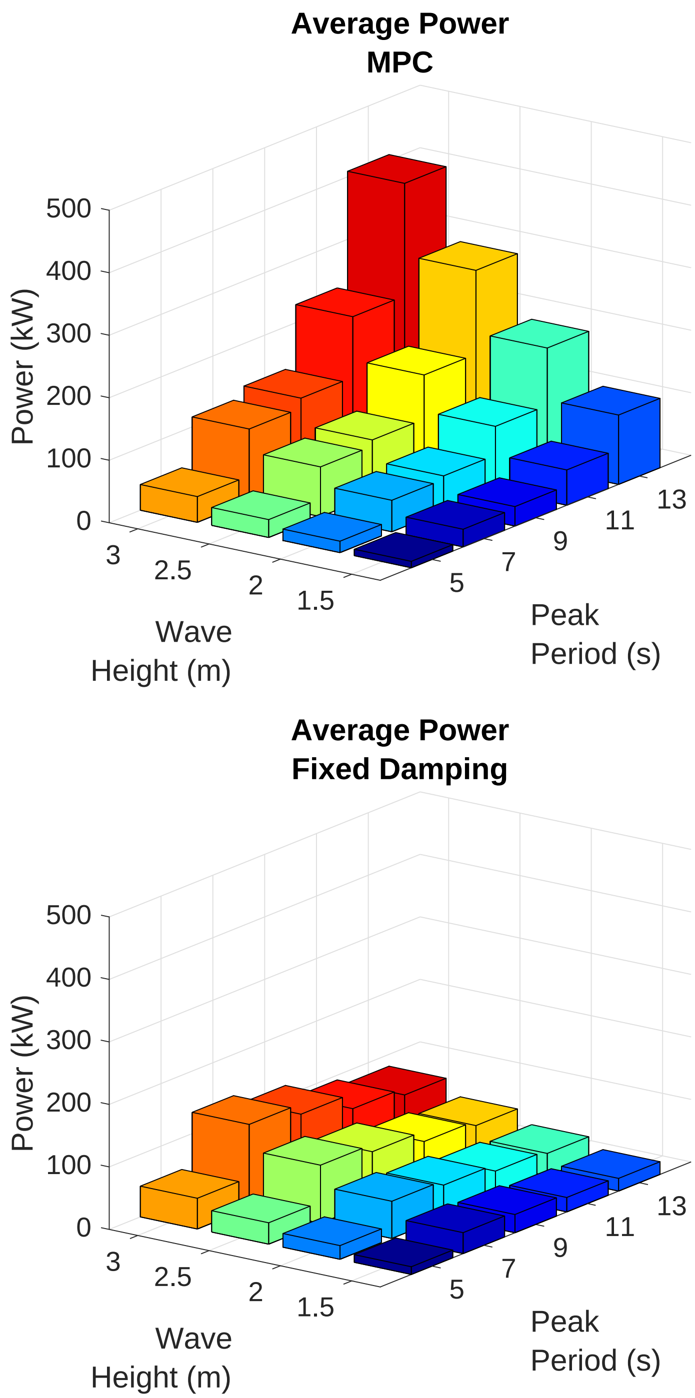

Figure 3.8: Average Power presented in terms of peak period and significant wave height. The bars are heat-map colored according to sea state energy (i.e., red is the highest energy sea state, blue is the lowest).

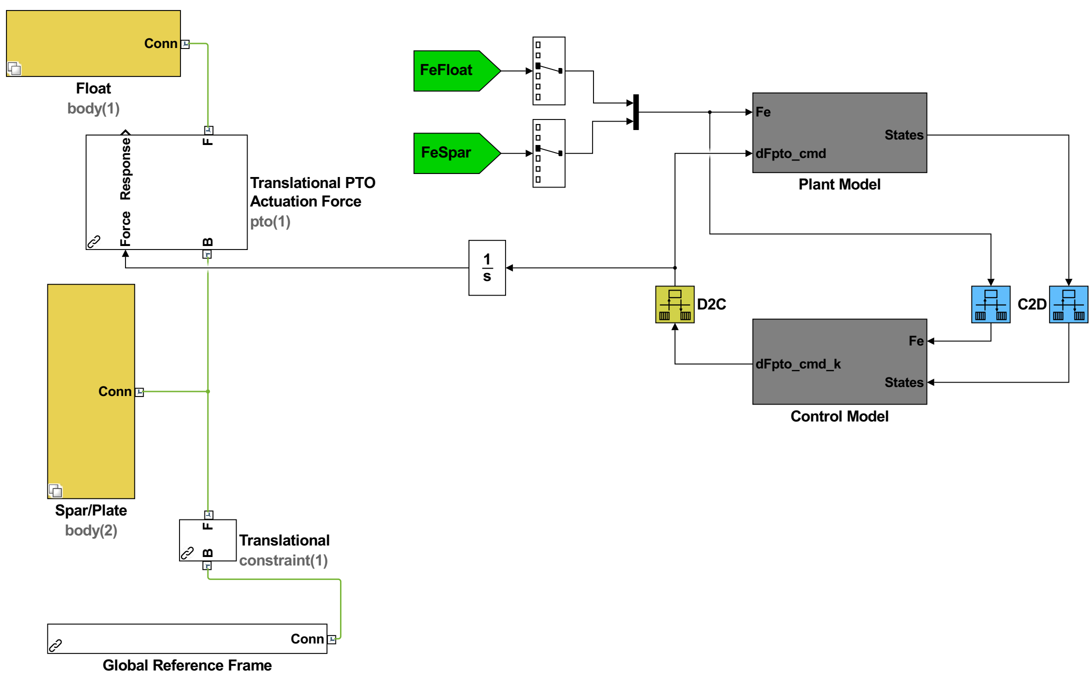

Figure 3.9: Simulink model for an integrated WEC-Sim with control.

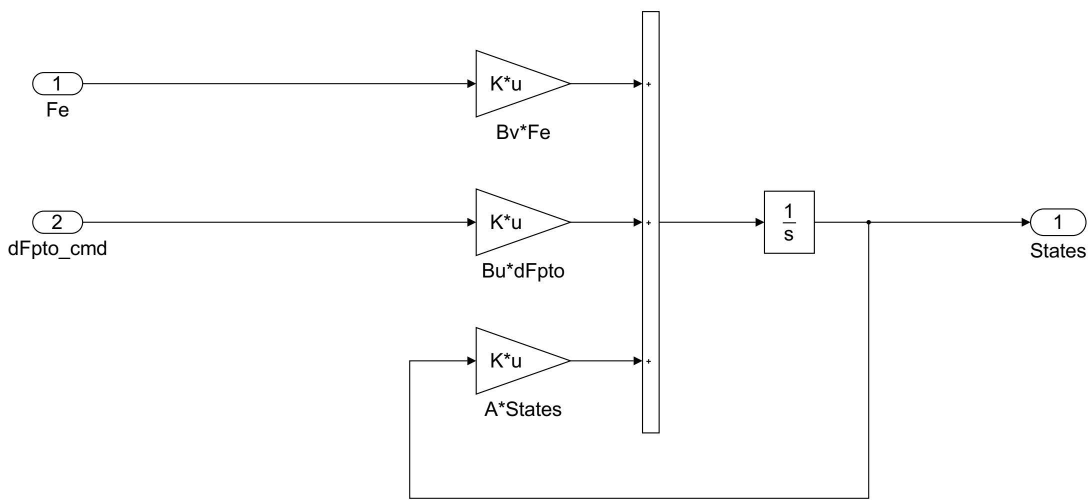

Figure 3.10: Plant model for control.

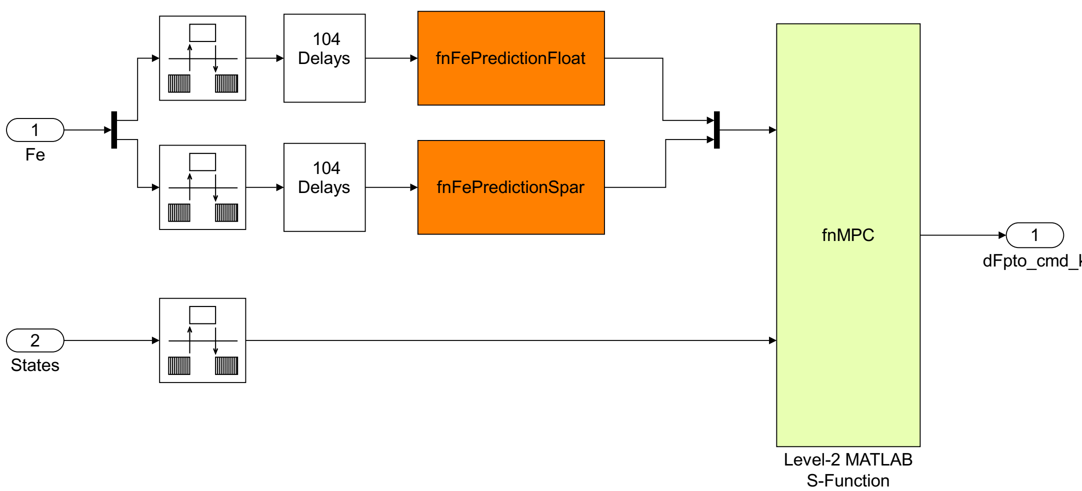

Figure 3.11: Control model.

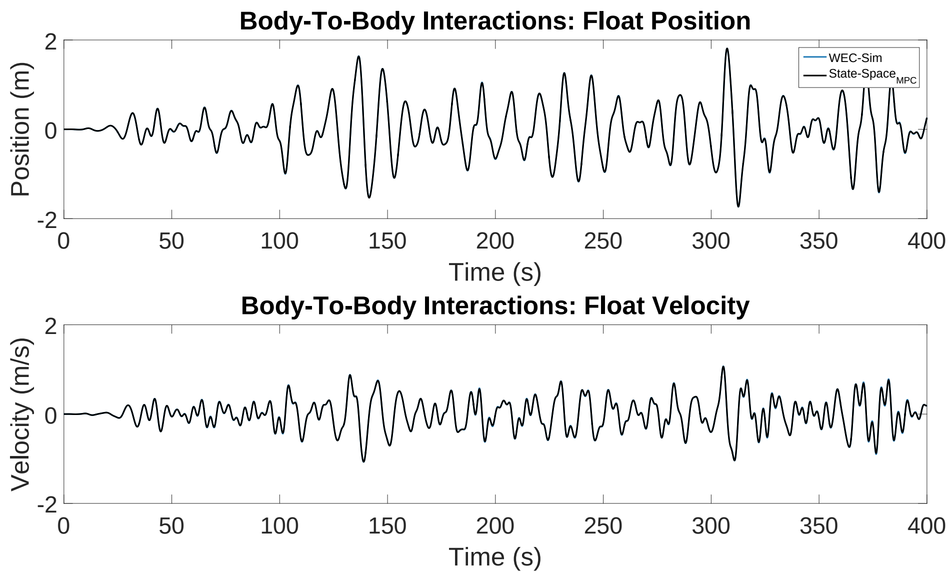

Figure 3.12: Float Comparison.

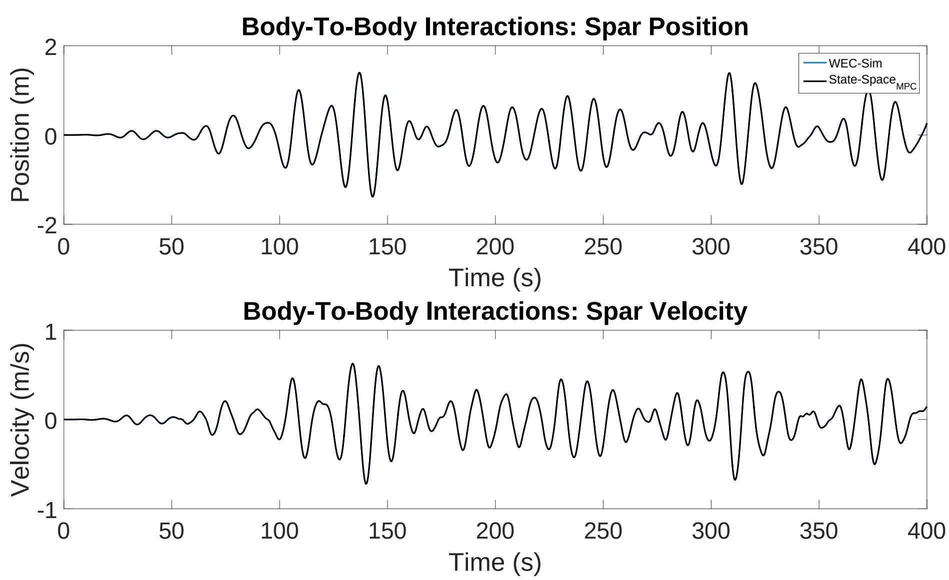

Figure 3.13: Spar Comparison.

Chapter 4: Conclusion

The goal of this research was to validate WEC-Sim against experimental data by testing two different wave energy converter devices. In addition, this study presented the development of model predictive control (MPC), latching & declutching, and linear Gaussian regulator (LQG) control strategies for WEC-Sim.

The first chapter presented a comparison between experimental performance of a prototype WEC (the CPwr SeaRay) and simulation results of the same WEC using WEC-Sim. The simulation of a complex three-body device with near-field interactions using linear hydrodynamics showed a good agreement in estimating the overall energy, estimating the total energy converted to within 24% (overprediction). One source of possible errors in the simulation are off-directional or spread waves from the real sea conditions. This issue was reduced by selecting trials with head-on waves and small spreading, but there is likely some deviation present. Furthermore, wave steepness and its impacts on hydrodynamics could be another possible discrepancy. There are perhaps some indications of this discrepancy in the non-consistency of predicted power for the aft float for low amplitude, high period waves, which have a very small steepness factor. Improvements can be achieved by using WEC-Sim with non-linear hydrodynamics, at the cost of increased computation time.

The second chapter presented a comparison between experimental performance of a prototype oscillating water column and simulated expected results of a point absorber in WEC-Sim. The study focuses on the responses of the oscillating water column for both regular and irregular waves. The former test presents both the amplitude and average power. The latter test discussed the average power, percent error in power, probability mass functions, and cumulative distribution functions. Focusing on the outlier events, the power errors in 95th percentile for valve positions at 80°, 71°, 62°, 53°, 44°, 35°, 26°, 17°, 8°, and 0° are -11%, -16%, -14%, -9%, -6%, 9%, 11%, 16%, 14%, and 23%, respectively. These results also consistent with the finding for percent error in power for irregular waves. Only when the valve is closed the error is high, the rest is 16% and lower. Furthermore, a states-space model that included the body-to-body interactions is very accurate when compared to the convolution approach used in WEC-Sim.

The third chapter presented the development of control strategies for wave energy converters. This chapter discusses multiple control strategies – such as linear spring damping, latching & declutching, linear quadratic Gaussian regulator (LQG), and model predictive control (MPC) – and how they work with wave energy converters. Some techniques such as latching and declutching are simpler to model and do not use reactive power while MPC, on the other hand, has a higher power capture improvement up to 500% compared to a fixed damping approach but requires the use of reactive power.

This research demonstrated the capability of WEC-Sim with body-to-body interactions using linear hydrodynamics. For early stage WEC development with a short simulation time, WEC-Sim showed a good predicted results even with complex bodies. This research also presented an example of power improvement up to 500% when model predictive control is implemented in WEC-Sim.

Bibliography

[1] Y. Yu, K. Ruehl, M. Lawson, and C. Michelen, "WEC-Sim wave energy converter SIMulator," 2015.

[2] Y. Yu, Y. Li, K. Hallett, and C. Hotimsky, "Design and analysis for a floating oscillating surge wave energy converter," in *Proceedings of OMAE 2014*, (San Francisco, CA), pp. 1–9.

[3] M. Lawson, Y. Yu, A. Nelessen, K. Ruehl, and C. Michelen, "Implementing nonlinear buoyancy and excitation forces in the WEC-sim wave energy converter modeling tool," in *Proceedings of OMAE 2014*, (San Francisco, CA), pp. 1–6, 2014.

[4] K. Ruehl, C. Michelen, S. Kanner, M. Lawson, and Y. Yu, "Preliminary verification and validation of WEC-sim, an open-source wave energy converter design tool," in *Proceedings of OMAE 2014*, (San Francisco, CA), 2014.

[5] Y. Yu, M. Lawson, K. Ruehl, and C. Michelen, "Development and demonstration of the WEC-sim wave energy converter simulation tool," in *Proceedings of the 2nd Marine Energy Technology Symposium*, (Seattle, WA, USA), pp. 1–8, 2014.

[6] "WaveDyn," 2013.

[7] "proteusDS," 2006.

[8] Z. Zhang, T. Brekken, K. Rhinefrank, A. Schacher, J. Prudell, E. Hammagren, and P. Lenee-Bluhm, "Adaptive damping power take-off control for a three-body wave energy converter," in *Energy Conversion Congress and Exposition (ECCE), 2013 IEEE*, pp. 321–328, Sept 2013.

[9] J. Falnes, *Ocean Waves and Oscillating Systems*. Cambridge University Press, 2002.

[10] K. Rhinefrank, A. Schacher, J. Prudell, E. Hammagren, A. von Jouanne, and T. Brekken, "Scaled development of a novel wave energy converter through wave tank to utility-scale laboratory testing," in *Power Energy Society General Meeting, 2015 IEEE*, pp. 1–5, July 2015.

[11] K. Rhinefrank, J. Prudell, and A. Schacher, "Development and characterization of a novel direct drive rotary wave energy point absorber MTS-IEEE oceans conference

proceedings," in *OCEANS 2009, MTS/IEEE Biloxi - Marine Technology for Our Future: Global and Local Challenges*, pp. 1–5, Oct 2009.

[12] K. Rhinefrank, A. Schacher, J. Prudell, J. Cruz, N. Jorge, C. Stillinger, D. Naviaux, T. Brekken, A. von Jouanne, D. Newborn, *et al.*, "Numerical and experimental analysis of a novel wave energy converter," in *ASME 2010 29th International Conference on Ocean, Offshore and Arctic Engineering*, pp. 559–567, American Society of Mechanical Engineers, 2010.

[13] K. Rhinefrank, A. Schacher, J. Prudell, E. Hammagren, Z. Zhang, C. Stillinger, T. Brekken, A. von Jouanne, and S. Yim, "Development of a novel 1: 7 scale wave energy converter," in *ASME 2011 30th International Conference on Ocean, Offshore and Arctic Engineering*, pp. 935–944, American Society of Mechanical Engineers, 2011.

[14] C.-H. Lee and J. N. Newman, "WAMIT user manual," 2016.

[15] A. ANSYS, "User manual (ver. 14.0)," 2012.

[16] "Nemoh a open source BEM," 2014.

[17] A. Henderson, J. Ahrens, C. Law, *et al.*, *The ParaView Guide*. Kitware Clifton Park, NY, 2004.

[18] A. Babarit, J. Hals, M. Muliawan, A. Kurniawan, T. Moan, and J. Krokstad, "Numerical benchmarking study of a selection of wave energy converters," *Renewable Energy*, vol. 41, pp. 44–63, 2012.

[19] J. Nolte and R. Ertekin, "Wave power calculations for a wave energy conversion device connected to a drogue," *Journal of Renewable and Sustainable Energy*, vol. 6, no. 1, p. 013117, 2014.

[20] W. Cummins, "The impulse response function and ship motions," tech. rep., No. DTMB-1661, 1962.

[21] S.-K. Song and J.-B. Park, "Modeling and control strategy of an oscillating water column-wave energy converter with an impulse turbine module," in *Control, Automation and Systems (ICCAS), 2015 15th International Conference on*, pp. 1983–1988, IEEE, 2015.

[22] H. Polinder, M. E. Damen, and F. Gardner, "Linear PM generator system for wave energy conversion in the AWS," *IEEE Transactions on Energy Conversion*, vol. 19, no. 3, pp. 583–589, 2004.

[23] D. R. Kiran, A. Palani, S. Muthukumar, and V. Jayashankar, "Steady grid power from wave energy," *IEEE Transactions on Energy Conversion*, vol. 22, no. 2, pp. 539–540, 2007.

[24] H. Polinder, B. C. Mecrow, A. G. Jack, P. G. Dickinson, and M. A. Mueller, "Conventional and TFPM linear generators for direct-drive wave energy conversion," *IEEE Transactions on Energy Conversion*, vol. 20, no. 2, pp. 260–267, 2005.

[25] B. Drew, A. R. Plummer, and M. N. Sahinkaya, "A review of wave energy converter technology," 2009.

[26] A. Muetze and J. Vining, "Ocean wave energy conversion-a survey," in *Industry Applications Conference, 2006. 41st IAS Annual Meeting. Conference Record of the 2006 IEEE*, vol. 3, pp. 1410–1417, IEEE, 2006.

[27] J. Ringwood, G. Bacelli, and F. Fusco, "Energy-maximizing control of wave-energy converters: the development of control system technology to optimize their operation," *IEEE Control Systems*, vol. 34, no. 5, pp. 30–55, 2014.

[28] J. Xie and L. Zuo, "Dynamics and control of ocean wave energy converters," *International Journal of Dynamics and Control*, vol. 1, no. 3, pp. 262–276, 2013.

[29] S. Salter, J. Taylor, and N. Caldwell, "Power conversion mechanisms for wave energy," *Proceedings of the Institution of Mechanical Engineers, Part M: Journal of Engineering for the Maritime Environment*, vol. 216, no. 1, pp. 1–27, 2002.

[30] A. Wright, W. Beattie, A. Thompson, S. Mavrakos, G. Lemonis, K. Nielsen, B. Holmes, and A. Stasinopoulos, "Performance considerations in a power take-off unit based on a non-linear load," in *Proc. 5th European Wave Energy Conference*, 2003.

[31] A. Kassem, A. Besheer, and A. Abdelaziz, "A linear quadratic gaussian approach for power transfer maximization of a point absorber wave energy converter," *Electric Power Components and Systems*, vol. 43, no. 8-10, pp. 1173–1181, 2015.

[32] T. Brekken, B. Batten, and E. Amon, "From blue to green [ask the experts]," *IEEE Control Systems*, vol. 31, pp. 18–24, Oct 2011.

[33] M. Starrett, R. So, T. Brekken, and A. McCall, "Development of a state space model for wave energy conversion systems," in *2015 IEEE Power Energy Society General Meeting*, pp. 1–5, July 2015.

[34] M. Starrett, R. So, T. Brekken, and A. McCall, "Increasing power capture from multibody wave energy conversion systems using model predictive control," in *Tech-*

nologies for Sustainability (SusTech), 2015 IEEE Conference on, pp. 20–26, July 2015.

[35] J. Falnes, *Ocean waves and oscillating systems: linear interactions including wave-energy extraction*. Cambridge university press, 2002.

[36] "Reference model project (RMP)," 2016.